Draft Manuscript for Review

Generation of arc and within-plate chemical signatures in collision zone magmatism: Quaternary lavas from Kurdistan Province, Iran

Journal:	*Journal of Petrology*
Manuscript ID:	JPET-Feb-12-0017.R3
Manuscript Type:	Original Manuscript
Date Submitted by the Author:	n/a
Complete List of Authors:	Allen, Mark; University of Durham, Earth Sciences Kheirkhah, Monireh; Geological Survey of Iran, Research Institute of Earth Sciences Neill, Iain; University of Durham, Department of Earth Sciences Emami, Mohamad; Geological Survey of Iran, Research Institute of Earth Sciences Mcleod, Claire; Durham University, Earth Sciences; University of Durham, Department of Earth Sciences
Keyword:	basalt, subduction, collision, Iran

Generation of arc and within-plate chemical signatures in collision zone magmatism: Quaternary lavas from Kurdistan Province, Iran

M.B.Allen[a*], M. Kheirkhah[b], I. Neill[a], M.H. Emami[b], C.L. McLeod[a,c]

[a]Department of Earth Sciences, Durham University, Durham, DH1 3LE, UK

[b]Research Institute for Earth Sciences, Geological Survey of Iran, Azadi Square, Meraj Avenue, Tehran, Iran

[c]Department of Earth and Atmospheric Sciences, University of Houston, 77204-5007, Texas, USA

* Corresponding author;

m.b.allen@durham.ac.uk; tel: +44 (0)191 3342344; fax: +44 (0)191 3342301

New elemental and isotopic analyses of Quaternary lavas from Kurdistan Province, western Iran, shed light on the nature of orogenic plateau magmatism during continental collision and the possible role of accessory minerals during mantle partial melting in this tectonic setting. The sampled lavas are from the Turkish-Iranian plateau within the Arabia-Eurasia collision zone. Compositions are typically basanite, hawaiite and alkali basalt, with minor rhyolite. Most of the basic samples from the Qorveh-Bijar region show elevated abundances of large ion lithophile elements (LILE) and light rare earth elements (LREE), e.g. 76 < La < 165 ppm, with steep REE patterns: 45 < La/Yb < 101. Two flows from Takab in the north of the study area have higher K_2O/Na_2O and Rb than the Qorveh-Bijar samples, but lower LREE and Ba. Sr-Nd isotope values for all the basic samples plot close to Bulk

Silicate Earth, with $^{143}Nd/^{144}Nd$ between 0.51263 and 0.51276, and $^{87}Sr/^{86}Sr$ between 0.70467 and 0.70600: this is similar to Quaternary alkali basalts from the Iran/Turkey borderlands to the northwest, but distinct from a more depleted source melting elsewhere in the same collision zone, for example at Mount Ararat and the Kars plateau (Turkey). Crustal contamination does not appear to be an important factor affecting composition. The range of chemical signatures suggests variable melting of at least two distinct sources. One inferred source produced melts with La/Nb ranging from ~3.5 to ~1.2, which is unusual for volcanic rocks that are otherwise coeval. We interpret this variation as the result of depletion of a K-richterite and rutile-bearing source during melting in the garnet stability field. The importance of this result is that the degree of the negative Nb anomaly and fractionation of LILE may depend on K-richterite and rutile in the source mineralogy, rather than simply the bulk abundances of incompatible trace elements in the source region. We infer the presence of phlogopite in a second mantle source, the melting of which produced the more potassic lavas from Takab. Lithosphere delamination or slab break-off mechanisms for triggering melting are problematic in the study area, as the lithosphere is reportedly ~150-200 km thick. Late Cenozoic extension has not been recognised, and so extension is unlikely as a cause of melting. The NW-SE alignment of volcanic centres, parallel to the regional structural grain, does imply a structural control at least on the final eruption site. Eurasian mantle lithosphere was probably metasomatised by fluids derived from Mesozoic-early Cenozoic subduction and the early stages of collision. More recent convergence has had the potential to cause further fluxing and melting of the re-fertilised lithosphere, with rapid magma ascent assisted by transcurrent motion along the orogen. It is also possible that the negative dT/dP section of the amphibole peridotite solidus was crossed as a result of

lithospheric thickening in the collision zone, i.e. compression melting rather than de-compression melting. Exhaustion of accessory phases may also help explain larger scale transitions from arc to within-plate chemistry in orogens, such as the Paleogene Arabia-Eurasia system, and the Mesozoic-Cenozoic magmatism of eastern China.

KEY WORDS*: basalt; collision; Iran; subduction;*

INTRODUCTION

This paper describes Quaternary syn-collision magmatism from Kurdistan (Kordestan) Province, western Iran, and compares it with other young centres generated within the Turkish-Iranian plateau. The plateau is part of the broader Arabia-Eurasia collision zone (Fig.1a-c). Such magmatism is a significant, regional aspect of continental collision zones (e.g. Pearce *et al.*, 1990; Keskin *et al.*, 1998; Williams *et al.*, 2004; Guo *et al.*, 2006; Prelević *et al.,*2008; Kirchenbaur *et al.* 2012), but the causes of the magmatism are not always understood. By looking at an example from an active collision it is possible to use constraints that are not available for ancient, inactive settings, such as the lithosphere thickness at the time of melt generation and the precise relations between magmatism and the regional deformation pattern.

The studied lavas have a wide variety of chemistries, but were erupted during a short time interval (~1 Myr) in the Quaternary, over a limited geographic area (outcrops strike in a NW-SE pattern for approximately 100 km; Fig. 1d). Lithosphere thickness is an important parameter: reported thicknesses of 150-200 km in the study area are highly unusual for a magmatic region, outside of plume/craton interactions (Priestley and McKenzie, 2006). The lavas represent an opportunity to look at the

effects of source composition, mineralogy, and melting conditions on magma chemistry in an active continental collision zone. They are also an example of young magmatism from the Iranian sector of the Alpine-Himalayan system, which is under-represented in the literature compared with areas to its east and west.

We address two main aspects in detail. Firstly, we focus on large ion lithophile element (LILE), rare earth element (REE), high field strength element (HFSE), and Nd-Sr isotope variations within the main suite of lavas. In particular, there is a compositional range from "spiky" trace element patterns on multi-element normalised plots ("spidergrams") to "smooth" patterns, typical of the global signatures of arc-like/subduction-modified and within-plate magmatism respectively (Wilson, 1989). We argue that the variations within the Kurdistan lava suite are controlled by minor phases in the source region, which are most likely to be amphibole (K-richterite) and rutile. This argument may be applicable to other, larger magmatic provinces which show a transition from arc to within-plate geochemical signatures, such as the Arabia-Eurasia orogen in the Paleogene, and the Mesozoic-Cenozoic magmatism of eastern China. Secondly, we address the cause of melting in Kurdistan Province, some 20-35 Ma after initial continental collision between Arabia and Eurasia. Our preferred melting model involves subduction and dewatering of Arabian passive margin sediments under the Eurasian plate, thereby fertilising, and triggering melting of, the Eurasian lithosphere. There may be a specific role for amphibole breakdown during convergence and lithospheric thickening. The Kurdistan magmatism therefore provides useful insights into processes that control the composition of the continental lithosphere.

GEOLOGICAL SETTING

Cenozoic continental collision has affected a vast area of Eurasia from the Pyrenees to Southeast Asia, collectively referred to as the Alpine-Himalayan system (e.g. Şengör, 1986). These collisions result from the subduction and eventual elimination of the Tethys Ocean northwards under the Eurasian active continental margin. Magmatism forms a prominent aspect of the collision zone evolution, and is attracting an increasing amount of study as it highlights processes operating within and beneath the lithosphere as plate convergence proceeds. Within the Mediterranean region, a wide range of magmatic rocks are known, including distinctive lamproite occurrences (Prelević *et al.,*2008; Tommasini *et al.,* 2011), commonly associated with late-stage orogenic extension. Further east, across eastern Anatolia (Turkey) and Iran, the Arabia-Eurasia collision is not associated with such major extension. Late Cenozoic magmatic rocks of the Turkish-Iranian plateau are varied in composition (e.g. Pearce *et al.,* 1990; Keskin *et al.,* 1998), ranging from alkaline basalts to more evolved sub-alkaline compositions. Ultrapotassic lavas are much rarer than the Mediterranean area. Collisional magmatism has also affected widespread if scattered parts of the Tibetan plateau (Williams *et al.,* 2004; Guo *et al.,* 2006).

Collectively, the magmatic rocks of the Alpine-Himalayan system allow us to understand the roles of processes such as slab break-off, lower lithosphere delamination and late stage orogenic extension ("orogenic collapse") in causing mantle melting. However, we are yet to understand the full range of causes of collision zone magmatism. There is a notable contrast between regions where late stage orogenic extension has occurred (around the Mediterranean), Iran (where it has not) and Tibet (where the youngest magmatism occurs north of the areas with most pronounced rifting).

Northward motion of Arabia in the Mesozoic and early Cenozoic was associated with subduction of Neo-Tethys under the southern margin of Eurasia (Berberian and King, 1981; Berberian *et al.*, 1982; Frizon de Lamotte *et al.*, 2011; Agard *et al.*, 2011). Arc and back-arc magmatism occurred across a wide area of SW Asia as a consequence of this subduction, with a marked flare-up in the Eocene, associated with back-arc extension, creating the Urumieh-Dokhtar Magmatic Arc (Kazmin *et al.*, 1986; McQuarrie *et al.*, 2003; Vincent *et al.*, 2005; Omrani *et al.*, 2008; Verdel *et al.*, 2011). A minor amount of magmatism took place southwest of the main magmatic front, within the Sanandaj-Sirjan Zone (Fig. 1c). Subduction-related magmatism waned dramatically in the late Eocene (Emami *et al.*, 1993), correlated by Allen and Armstrong (2008) with the onset of Arabia-Eurasia continental collision at about 35 Ma. Other estimates put initial collision later, e.g. early Miocene, 20 Ma (Okay *et al.*, 2010). A possible explanation for these different estimates is that initial collision at 35 Ma involved thin continental crust at the northern side of the Arabian plate, and thicker crust only entered the collision zone after 10-15 Myr of further convergence (Morley *et al.*, 2009; Ballato *et al.*, 2011).

Collision between the Arabian and Eurasian plates is active, with present ~north-south plate convergence in the order of 20 mm/yr at longitude 50^{o}E (Vernant *et al.*, 2004). This is an important constraint: collision was not an instantaneous event, but is a process that takes tens of millions of years and involves long-term shortening and thickening of the crust and the mantle lithosphere, both by internal shortening and by underthrusting of the Eurasian margin by the Arabian plate.

Active deformation is not evenly distributed within the collision zone (Jackson *et al.*, 1995), but is focussed on the mountain ranges at the northern and southern margins. The intervening Turkish-Iranian plateau (Fig. 1a&b) is not undergoing major

active crustal thickening (e.g. Berberian and Yeats, 1999; Allen *et al.*, 2011a). Earlier, collision-generated thickening of the Turkish-Iranian plateau is indicated by both present Moho depths (commonly 45 – 65 km; Paul *et al.*, 2010) and the record of Cenozoic compressional deformation (Agard *et al.*, 2005; Morley *et al.*, 2009). Pre-collisional rocks include Cretaceous marine strata (National Iranian Oil Company, 1978), indicating that these crustal thicknesses were achieved during the Cenozoic collision, presumably as the result of crustal and lithospheric shortening. The Turkish-Iranian plateau is now typically 1.5-2 km in elevation in western Iran. It is not clear when the compressional deformation stopped in each part of the present plateau, but across many regions it appears to have been in the Pliocene-Quaternary, i.e. since ~5 Ma (Allen *et al.,* 2011a).

Magmatism has occurred intermittently within SW Eurasia between the Oligocene and the present day, across much of the region north of the original Arabia-Eurasia (Zagros) suture (Emami *et al.*, 1993), and more rarely to the south, e.g. Karacadag in southeastern Turkey (Lustrino *et al.*, 2010). Volcanism has occurred predominantly within the Turkish-Iranian plateau, particularly since ~10 Ma across the Kars plateau of eastern Turkey and neighbouring areas in Armenia and northern Iran (Fig. 1a; Keskin *et al.*, 1998). Many centres are late Pliocene or Quaternary in age (Yilmaz *et al.*, 1998; Davidson *et al.*, 2004; Bridgland *et al.*, 2007; Walker *et al.*, 2009; Shabanian *et al.*, 2009; Allen *et al.*, 2011b; Fig. 1a&b). Both large, evolved composite volcanoes (e.g. Ararat, Sabalan, Sahand) and much smaller, basic, fields are present. Pliocene-Quaternary magma types range from calc-alkaline to alkaline and even shoshonitic, with trace element characteristics resembling both magmas formed at active continental margins and those from within-plate scenarios (Pearce *et al.*, 1990; Keskin *et al.*, 1998; Parlak *et al.*, 2001; Davidson *et al.*, 2004; Liotard *et al.*,

2008; Walker *et al.*, 2009; Kheirkhah *et al.*, 2009; Ahmadzadeh *et al.*, 2010; Dilek *et al.*, 2010; Saadat and Stern, 2011). Some centres are potassic or even ultrapotassic (Aftabi and Atapour, 2000; Moayyed *et al.*, 2008; Ahmadzadeh *et al.*, 2010), such as Eslamy (Fig. 1b). High silica adakite compositions have also been reported, which are of uncertain geodynamic significance (Jahangiri, 2007; Omrani *et al.*, 2008).

The nature and origins of this Quaternary syn-collision magmatism are still debated, including the issue of why there has been an apparent flare-up 20-30 Myrs after initial collision and the end of oceanic subduction under this part of Eurasia (Keskin, 2007; van Hunen and Allen, 2011).

The chemical variation displayed by the Pliocene-Quaternary volcanic rocks has led to a variety of postulated source regions and melting regimes. Pearce *et al.* (1990) suggested lithospheric delamination as an overall trigger for lithospheric partial melting in the region. Keskin (2003) invoked break-off of the subducting Neo-Tethyan oceanic slab beneath Eurasia as a potential trigger for the concentration of magmatism in eastern Anatolia. Both mechanisms may be applicable (Keskin, 2007).

The study area lies within the Sanandaj-Sirjan Zone (Fig. 1c), which is a Gondwana-derived block that accreted to other Iranian crustal blocks during the destruction of Palaeo-Tethys (Şengör *et al.*, 1988; Stampfli and Borel, 2002). The Sanandaj-Sirjan Zone was at the southwest margin of Eurasia during the Mesozoic-early Cenozoic subduction of Neo-Tethys, but the magmatic record of this region is relatively small, perhaps implying periods of slow and/or flat subduction. Lower Cretaceous limestones cover extensive areas of the Sanandaj-Sirjan Zone (National Iranian Oil Company, 1978), indicating little magmatism, elevations below sea level and near normal crustal thickness at this time.

Crust of the Sanandaj-Sirjan Zone has been thickened to ~65 km (Paul *et al.*, 2010), presumably as the result of shortening and thickening after the initial collision (Agard *et al.*, 2005). Lithosphere thickness is ~150-200 km (Priestley and McKenzie, 2006), apparently thickening from northwest to southeast across the study area containing Quaternary volcanism (Fig. 1b). These values are derived from a global study of shear wave velocity gradients, with a quoted resolution of 400 km, so there is no detailed resolution on the scale of the study area.

With the exception of the basic volcanics analysed here, there is little post-Eocene magmatism in the vicinity of the study area, although lower-middle Miocene andesites crop out north of Takab (Daliran, 2008), and upper Miocene acidic volcanics crop out ~30 km west of the basic volcanics (Fig. 1d; Boccaletti *et al.*, 1976).

At a poorly-constrained time in the late Cenozoic, compressional deformation ceased across the Sanandaj-Sirjan Zone, and it became part of the Turkish-Iranian plateau; crustal thickening migrated southwards through the Zagros towards the margin of the collision zone (Allen *et al.*, 2004; Mouthereau, 2011; Nissen *et al.*, 2011). The absence of seismogenic thrusting and lack of internal shortening in the GPS-derived velocity field indicate that upper crustal shortening is not active in the study area (Vernant *et al.,* 2004; Nissen *et al.,* 2011). Nor is there a local record of recent compressional deformation in the geomorphology and bedrock geology: both the studied lavas and the underlying Pliocene-Quaternary fluvial/lacustrine sediments that they overlie are sub-horizontal. However, nor is there a record of late Cenozoic extension. At the larger scale, Iran has not experienced either the style of narrow rifting that effects southern Tibet or the more widespread extension of some orogenic belts around the Mediterranean (e.g. Dewey, 1988).

SAMPLES AND ANALYTICAL TECHNIQUES

Samples

Lavas are distributed along a rough NW-SE trend for ~100 km, northwest of the city of Hamadan (Fig. 1d). This trend is parallel to the main regional structural grain. Isolated outcrops are remnants of lava flows that were erupted over an intramontane fluvial-lacustrine basin within the Turkish-Iranian plateau (Zahedi and Hajian, 1985). There was no significant deposition that post-dated the flows. This basin is currently being dissected by external drainage, creating 3D exposures of the lavas. The three main outcrop centres are near the towns of Takab, Bijar and Qorveh. Samples are from lava flows near Takab and Bijar, and lava flows or scoriaceous bombs within cinder cones at Qorveh (Fig. 1d). Individual flows are several 10s of metres thick. The cinder cones are distributed over the lava flows and so appear to be the youngest phase of magmatism in the region. Cone morphology is fresh; craters are preserved, suggesting the relative youth of the features.

Boccaletti *et al.* (1976) recorded six Quaternary K-Ar ages from the Qorveh and Bijar centres in the range 1.3 ± 0.08 to 0.5 ± 0.15 Ma, with errors based on estimated ^{40}Ar concentrations. Samples had loss-on-ignition (LOI) values of 0.9-2.3%, indicating that they may have undergone a small degree of sub-solidus alteration. No further analytical details are available. There are no radiometric ages available for the lavas nearest Takab (Fig. 1d), but as the geomorphology of the lava outcrop is the same as at Qorveh and Bijar we infer a similar Quaternary age.

The groundmass of the basic lava flows and scoria contains clinopyroxene, olivine, opaque minerals and nepheline. There are abundant clinopyroxene

microphenocrysts, and rare clinoproxene and olivine phenocrysts up to 1-2 mm across. Biotite is an accessory phase in some samples. The scoria samples are highly vesicular. Rhyolite flows contain oligoclase and amphibole phenocrysts in a glassy groundmass. Samples are generally fresh, although some contain clay-filled vesicles, removed during sample preparation. Some of the olivine phenocrysts are chloritised. Sample TBQ5.4 is different from the other basic samples, with abundant plagioclase in the groundmass.

Analytical techniques

Major elements for 34 samples were analysed by a PANalytical Axios Advanced XRF spectrometer, at the Department of Geology, University of Leicester. Major elements were analysed on fused glass beads prepared from ignited powders. Sample to flux ratio was 1:5, with an 80% Li metaborate: 20% Li tetraborate flux. Full analytical procedures are in Tarney and Marsh (1991). Samples were analysed for trace elements by Inductively Coupled Plasma Mass Spectroscopy (ICP-MS), using a Perkin Elmer-Sciex Elan 6000 in the Department of Earth Sciences at Durham University, following a standard nitric and hydrofluoric acid digestion (Ottley *et al.*, 2003). Analyses for element standards are given in Electronic Appendix 1, via the Journal of Petrology website at http://www.petrology.oupjournals.org. The accuracy of the results can be inferred from measured values of these standards. Typical analytical precision, estimated from replicate measurements of international standard NBS688, was better or equal to 3% RSD.

Preparation of whole rock powders for Sr and Nd isotope analysis was carried out at the Arthur Holmes Isotope Geology Laboratory (AHIGL) in the Department of Earth Sciences at Durham University, UK. For detailed sample preparation and

chemical separation techniques, see Dowall *et al.* (2003). Powders were digested in a standard HF-HNO_3 procedure and run through 1 ml pipette tips containing several drops of dilute Sr-spec resin to collect the Sr-bearing fraction. The high field strength element (HFSE) and rare earth element (REE)-bearing fraction from these columns was run through 10 ml Bio-Rad polypropylene columns containing 1 ml of Bio-Rad AG1-X8 200-400 mesh anion-exchange resin. Neodymium was collected as part of a total rare earth element fraction. Samples were analysed using a Thermo Electron Neptune Multi-collector Plasma Mass Spectrometer (MC-ICP-MS) at AHIGL following the analytical procedure detailed by Dowall *et al.* (2003) and Nowell *et al.* (2003). All samples were run during a single analytical session for each isotope system. The average $^{87}Sr/^{86}Sr$ of the international standard NBS987 was 0.710257±0.000013, corresponding to an analytical uncertainty of 18.6 ppm (2σ, n=12), and comparable to a preferred value of 0.710240. The average $^{143}Nd/^{144}Nd$ of a combination of pure and Sm-doped J&M internal Nd standards was 0.511114±0.000011, giving an analytical uncertainty of 22.4 ppm (2σ, n=15), and comparable to a preferred value of 0.511110. No corrections were applied to these results.

RESULTS

Major and trace element data and Sr-Nd isotope values are presented in Table 1. The majority of the samples have LOI <1%, consistent with the overall freshness of the flows, but a couple of the flows with LOI > 1% are associated with variable LILE concentrations, e.g. lower K_2O than otherwise equivalent samples (Table 1). Silica contents range from 44 to 66%, but only one of the samples is rhyolitic; the second highest SiO_2 content is <51%. Boccaletti *et al.* (1976) also reported rare rhyolites,

such that the distribution of compositions is bimodal (Fig. 2). Samples from cones are not separated from samples from flows on the geochemical plots; the cone samples show the full range of chemical variation.

On the total alkali versus silica diagram (Fig. 2a) most samples plot within the alkali field and are sodic basanites and hawaiites with $Na_2O > K_2O$. Na_2O is typically ~4.5% and K_2O ~3% (Table 1). Sample TBQ5.4 is a basalt from a flow 20 km southwest of Bijar (Fig. 1d), geographically distinct from flows to the southeast, and with a distinctive chemistry: it is the only sample with $Na_2O + K_2O$ <5% (Fig. 2a). However, another sampled flow from this locality, TBQ5.11, shows no difference from the main range of the Qorveh-Bijar samples. The two samples from the outcrop closest to Takab (Fig. 1d) are hawaiites (TBQ1.1 and TBQ1.2). They have higher K_2O and lower Na_2O than the rest of the samples; from this pair, sample TBQ1.1 is the only one of the entire sample set that is truly potassic, with $K_2O > Na_2O$.

The most basic samples have MgO >10%, Ni >300 ppm, Cr >350 ppm and mg# ~70, indicating near primary melt compositions. Major element fractionation trends for the entire sample suite are not well defined, with clustering of samples for example in the plot of MgO v SiO_2 (Fig. 2b); the sample set does not therefore look like a single fractionation trend from a unique parental composition. Nevertheless, FeO_T, CaO and TiO_2 broadly decrease with increasing SiO_2, consistent with the fractionation of an assemblage of olivine ± pyroxene ± titanomagnetite (Fig. 2).The two hawaiites from Takab have higher SiO_2 and lower CaO and TiO_2 than the bulk of the samples (Fig. 2).

Y and Dy/Yb show no clear correlation with SiO_2, except for the most acidic sample (TBQ15.1), which contains 12 ppm Y, compared to ~20-30 ppm Y in the other samples. This finding implies that amphibole fractionation is not responsible for

chemical variation in the basic samples, and that the cryptic amphibole fractionation that commonly takes place in active arcs (Davidson *et* al., 2007) does not apply to the studied lavas. Dy is more compatible than Yb in amphibole, so amphibole crystallisation should alter the ratio of these elements during magmatic differentiation (Klein *et al.*, 1997).

Representative primitive mantle-normalised variation diagrams (spidergrams) are presented in Fig. 3a&b. Patterns are normalised to the primitive mantle composition of Sun and McDonough (1989). Rare earth element (REE) patterns on Fig. 3c&d show varying enrichment of the light REE (LREE), with smaller variation of the heavy REE (HREE). Patterns in the spidergrams are typically steep, with enrichment of the large ion lithophile elements (LILE) over the high field strength elements (HFSE) and steep REE patterns: $45 < La/Yb < 101$, except for the Takab hawaiites already noted, where La/Yb ~20, and sample TBQ5.4 where La/Yb = 19. With these same three exceptions, basic samples are highly enriched in the more incompatible elements (e.g. $76 < La < 165$ ppm). All samples show a negative Nb-Ta anomaly on the spidergrams, which is usually understood to imply the presence of a subduction-modified component in the mantle source and/or crustal contamination (e.g. Pearce and Peate, 1995). However, La/Nb ratios are highly variable, from ~1.2 to >3 (Figs. 4 and 5). Lower La/Nb is associated with lower LILE concentrations, less intra-LILE variation and flatter REE patterns (Fig. 3a; Fig. 5a). There is no clear variation between the La/Nb ratio and major element or compatible trace element composition, e.g. no clear sign of a trend in the plot of La/Nb v Ni (Fig. 5b).

For all samples $(Ba/Rb)_N > 1$, with the exception of the two lavas from near Takab (Fig. 3b). Some of the samples with the steeper spidergrams show a negative Sr anomaly. All samples show a negative anomaly at Ti, which can be expressed as a Ti

anomaly, Ti/Ti*, where Ti* represents the extrapolated value of Ti based on the abundances of the elements on either side of Ti on the spidergrams (Fig. 6).

Results for the nineteen samples analysed for Sr and Nd isotopes are plotted on Fig. 7a. All but one of the $^{143}Nd/^{144}Nd$ values range between 0.51263 and 0.51276, and $^{87}Sr/^{86}Sr$ ranges between 0.70467 and 0.70600, thus placing the sample array close to bulk silicate Earth (BSE) on the $^{143}Nd/^{144}Nd$ versus $^{87}Sr/^{86}Sr$ plot.

DISCUSSION

Evaluation of possible crustal contamination

It is worth discussing the possible effects of crustal contamination before trying to unravel source region characteristics and melting histories. Most of the samples are basic, with MgO > 8%. MgO values of >10% are common, and the basic lavas are uniformly silica undersaturated. Therefore bulk contamination involving crustal materials (or extensive fractionation) is unlikely. Trace element patterns on the spidergrams do show distinctive spikes associated with continental crust, especially peaks at Ba, Th and La. However, the abundances of these elements are far higher than in bulk continental crust (Rudnick and Fountain, 1995), such that simple mixing of a primitive, depleted magma with typical crust is not a viable mechanism for generation of the observed trace element patterns. On trace element plots such as La/Nb v La/Yb (Fig. 5a), there is no trend between the Kurdistan data array and global average crustal compositions, or representative individual samples from along the Alpine-Himalayan system.

Rhyolite TBQ15.1 has an $^{87}Sr/^{86}Sr$ value similar to the basic lavas nearby (Fig. 7a), such that there are no isotopic grounds for deducing assimilation of crust in this evolved lava. Two samples (TBQ1.2 and TBQ5.4) show a modest shift towards

higher $^{87}Sr/^{86}Sr$ values, which could reflect limited crustal contamination. They also fall close to published values for Tendürek volcano, in the eastern Turkey/northwest Iran borderlands (Kheirkhah *et al.*, 2009; Fig. 7a). One of these samples, TBQ1.2, is from the pair of hawaiite lavas from Takab, which show other distinctions from the main set from Qorveh and Bijar. The other, TBQ5.4, is also distinctive in terms of its trace element characteristics and petrography.

Overall, there is no clear correlation between $^{87}Sr/^{86}Sr$ and SiO_2, or $^{87}Sr/^{86}Sr$ and mg#, which would be expected if crustal contamination occurred with increasing fractionation (Fig. 7b). Trace element abundances, and trace element ratios such as Ce/Pb which might be sensitive to crustal contamination do not correlate with $^{87}Sr/^{86}Sr$ values (Fig. 7c), although, uniquely, rhyolite TBQ15.1 does have a lower value for Ce/Pb than other samples.

Mixing of a depleted MORB mantle source (DMM) (Workman and Hart, 2005) and 1-2% Tethyan flysch sediment (Prelević *et al.* 2008) comes close to the Kurdistan array of Nd-Sr isotopic compositions (Fig. 7a), but does not overlap. However, as noted above, simple mixing of MORB-like magma and crust does not work on trace element grounds. Other, more enriched, sediment compositions such as GLOSS (Global Subducting Sediment; Plank and Langmuir, 1998) produce mixing lines further away from the data array, and so are even less likely as crustal contaminants (Fig. 7a). Both mixing lines shown are relatively linear because of the similar Sr/Nd ratios of the end members in the calculations,

From the above arguments, we conclude that crustal contamination is not a significant process governing the geochemical composition of the main Qorveh-Bijar sample set. Later, we discuss the possibility that a small component of sedimentary origin is involved in the source region of the magmas.

Incompatible trace and minor element patterns

Almost all the spidergrams show enrichment in highly incompatible elements relative to mid ocean ridge basalt (MORB) and typical ocean island basalt (OIB) (Fig. 3). Different patterns are evident within the overall sample set. The samples from near Qorveh and Bijar show a variation from steeply enriched and spiked patterns, typified by TBQ19.1, to less steep and smoother patterns, typified by TBQ14.1 (Fig. 3a). There is pronounced variation in the relative abundances of Nb and Ta, further picked out by the plot of La versus Nb (Fig. 4). La/Nb ratios vary between ~1.2 and ~3.5, such that while all samples possess a negative Nb-Ta anomaly, its magnitude is one of the parameters that varies the most between samples. Such variation in La/Nb ratio is unusual in coeval basic magmatic suites, and is typically not seen in other centres from the Turkish-Iranian plateau (Fig. 4), with the exception of Damavand volcano in the Alborz mountains of northern Iran (Fig. 1a&b). La/Nb ratios in basic magmatic suites are not typically affected by the degree of partial melting or fractionation. La/Nb ratios of the Kurdistan sample set also do not correlate with $^{87}Sr/^{86}Sr$ values (not shown), suggesting that the variation in the trace element chemistry is unrelated to any isotopic heterogeneity in the source.

La/Nb does correlate positively with La/Yb, i.e. the steepest REE traces and spidergrams occur at the highest La/Nb ratios (Fig. 5a). The steep REE patterns and low HREE abundances of all the Qorveh and Bijar lavas are consistent with melting in the garnet stability field (i.e. depths of >80 km), with increased degrees of melting producing the less steep REE patterns. This is addressed more quantitatively later.

Variations between the LILE become more subdued as La/Nb decreases, such that the spidergrams vary between the pronounced spikes in LILE shown by TBQ19.1

to the much more smooth patterns of TBQ14.1 (Fig. 3a). Therefore within the sample set there is a variation from the distinctive spikes and negative Nb-Ta anomalies normally associated with subduction-related modification of mantle sources (Pearce and Peate, 1995), towards the smoother patterns and lower La/Nb ratios more typical of within-plate magmatism (Sun and McDonough, 1989). This compositional range is also visible in the plot of La/Nb v La/Yb, (Fig. 5a), where the main Qorveh-Bijar array shows a rough trend towards typical OIB values, without any sample falling close to OIB. The lowest La/Nb ratios and smoothest spidergrams occur in samples from the cinder cones at Qorveh, i.e. post-dating the flows, and are apparently from the last stage of magmatism.

There is no clear correlation between La/Nb and compatible trace elements such as Ni (Fig. 5b) or major element indicators of fractionation such as MgO or mg# (not shown), such that the variation in La/Nb does not appear to result from fractionation and/or contamination processes.

Samples from Qorveh and Bijar show a positive correlation between their Nb/Ta and Zr/Hf ratios, consistent with these elements being fractionated from each other during magma production (Fig. 8). Garnet in the residue can fractionate Zr/Hf in melts, with higher Zr/Hf generated at smaller melt fractions (Pfänder *et al.*, 2007): the higher Zr/Hf samples from Kurdistan possess higher La/Yb ratios, consistent with their origin by the smallest degree of partial melting. However, residual garnet only controls the Nb/Ta ratio if the source has an unusually low Zr/Hf ratio (~27), consistent with depleted mantle (Pfänder *et al.*, 2007): this seems unlikely for the source region of the Kurdistan lavas, given that their Sr-Nd isotopic signature does not indicate a depleted source region. Amphibole in the mantle source could explain the observed variation in Nb/Ta ratios (Fig. 8), but would require unusual amphibole

compositions, as even high mg# amphiboles (mg# > 70) have $D_{Amph/L}$(Nb/Ta) in the range 0.8 to 1.4, and $D_{Amph/L}$(Nb/Ta) < 1 would be necessary (Tiepolo *et al.*, 2000; Foley *et al.*, 2002). Lower mg# amphiboles have $D_{Amph/L}$(Nb/Ta) >1.4, and so produce lower Nb/Ta in corresponding melts (Tiepolo *et al.*, 2000; Foley *et al.*, 2002). Rutile is a candidate mineral, as $D_{Rutile/L}$(Nb/Ta) ~0.45-0.6 (Foley *et al.* 2002; Schmidt *et al.*, 2004; Foley, 2008), such that rutile in the source would raise Nb/Ta in corresponding melts.

The two hawaiite samples from Takab are distinct from the main Qorveh and Bijar compositions. They show flatter spidergrams than the main sample set, with higher HREE and lower LREE). The LILE of the Takab samples contrast with the samples from Qorveh and Bijar. Ba/Rb ratios are lower for these Takab samples than those to the south; they are depleted in Ba and enriched in Rb compared with the Qorveh-Bijar samples. K_2O concentrations are among the highest of any of the samples (K_2O = 3.1-3.3 wt.%). On a plot of Rb/Sr v Ba/Rb (Fig. 9), the Takab hawaiites plot on a high Rb/Sr trend associated with phlogopite in the mantle source, whereas the bulk of the samples from Qorveh and Bijar follow a low Rb/Sr, high Ba/Rb trend typical of an amphibole-bearing source (Furman and Graham, 1999; Tommasini *et al*., 2011). There is a positive correlation between Ba/Rb and La/Nb and Ba/Rb and La/Yb for the Qorveh-Bijar samples (not shown), such that the strongest amphibole signature matches the most pronounced subduction signature and the lowest degree of partial melting.

One basalt sample from Bijar (TBQ5.4) is significantly different from all the others in this study, having lower abundances of most incompatible elements, but higher HREE concentrations (Fig. 3b). Its major and trace element composition closely resembles basic lavas from Ararat and Tendürek volcanoes to the northwest

(Notsu *et al.*, 1995; Kheirkhah *et al.*, 2009), although its incompatible trace element abundances lie between the ranges recorded from these centres (e.g. Fig. 4). TBQ5.4 has higher $^{87}Sr/^{86}Sr$ than any other basic sample in this study (0.705998). Its Sr-Nd isotopic composition is similar to published values from Tendürek (Fig. 7). We are cautious about drawing too many conclusions from one sample, but we conclude that it may be the product of shallower, more extensive melting (consistent with the low LREE/HREE ratios and relatively high HREE), coupled with either a degree of crustal contamination or a more isotopically enriched source to elevate the $^{87}Sr/^{86}Sr$ value.

Models for melting conditions

Conditions clearly became suitable for melting the mantle beneath Kurdistan in the late Cenozoic, but the precise trigger for melting is unclear, and is discussed in the next section.

It is not possible to produce the observed compositions by simple mixing of two end members, such as the highest and lowest La/Nb samples. Trace element patterns such as Zr/Y v Nb (Fig. 10) show that the high Nb samples do not simply fall at one end of a linear array. Other elements exhibit similar behaviour; the high Nb samples are also associated with high Rb, for example (Fig. 10). The arrays on Fig. 10 are better explained by increasing partial melting reducing both Zr/Y and Nb (and Rb), followed by a number of samples where the behaviour of Nb and Rb changes from being compatible in the source to incompatible.

Fig. 11 shows the results of non-modal batch melting models for Gd/Yb v Dy/Yb, to constrain the melting regime, and in particular to address the question of whether garnet is present in the source. We have used spinel and garnet lherzolite mineralogies and modes, following Thirlwall *et al.* (1994), with the addition of minor

amounts of amphibole and rutile. Distribution coefficients are taken from Kelemen *et al.* (1993), Tiepolo *et al.* (2003) and Foley (2008). Full parameters are shown in Table 2. Several different source compositions are shown for comparison. A mixture of inferred depleted MORB mantle source (DMM) (Workman and Hart, 2005) and 2% Tethyan flysch sediment (Prelević *et al.* 2008) satisfies Nd-Sr isotopic constraints (Fig. 7a) and produces a good fit to the Kurdistan ratios at ranges of 0.1-10% melting of a garnet lherzolite source. Other sediment additions to the source, such as GLOSS, would produce isotopic signatures further from the Kurdistan data array (Fig. 7a), and so are not considered.

A starting composition of an amphibole-garnet peridotite from the Massif Central (Fréménias *et al.* 2004) produces a similar curve and match to the data. Modelled abundances of the REE are too low by a factor of five, however, suggesting that the real source is more fertile for these elements. We note that hornblendite veins and xenoliths have been reported from lherzolites within and beyond the Tethyan realm that have appropriate REE values (~3 ppm for Gd and Dy, and ~2 ppm for Yb; e.g. Orejana *et al.* 2006; Choi *et al.* 2007). Other possible sources, such as DMM without the sediment addition, produce melting curves that have too low Gd/Yb and Dy/Yb to match the observed data.

The melt curves are consistent with garnet being present in the source for the great majority of the Qorveh-Bijar samples (Fig. 11). Uniquely, sample TBQ5.4 falls closer to the melting curves for spinel lherzolite mineralogy, and similar to the melt models inferred for larger volcanic centres in the Turkey/Iran borderlands such as Ararat and Tendürek (Sen *et al*. 2004; Kheirkhah *et al.* 2009). As the crust in the Sanandaj-Sirjan Zone commonly reaches ~60 km (Paul *et al.,* 2010), it is not surprising that melting typically takes place below the spinel stability field.

In summary, the composition of most of the Qorveh and Bijar samples is consistent with melting in the garnet stability field, i.e. depths >80 km for peridotite, consistent with the high LREE/HREE ratios and low abundances of the HREE. As these lavas make up the vast majority of the sample set, we now focus on their petrogenesis in more detail.

Possible roles of accessory minerals

The variation of Nb and Ta, with respect to other trace elements is one of the most distinctive features of these rocks, and any explanation for their origin must account for their behaviour. Rutile has high partition coefficients for Nb and Ta (e.g. D_{Nb} ~15 for basaltic melts; Schmidt *et al.*, 2004, or >100; Foley *et al.*, 2000), and it has long been implicated as the origin of negative Nb and Ta anomalies in subduction-influenced settings (e.g. Foley and Wheller, 1990). Rutile was picked out as a source region control on high and low Nb basalts during arc magmatism at Turrialba volcano, Costa Rica (Reagan and Gill, 1989), with high Nb compositions implying the absence of rutile in the source. However, the Turrialba lavas do not show significant variation in highly incompatible elements other than Nb (Ta was not analysed), consistent with rutile having very low partition coefficients for these elements (Foley *et al.*, 2000). In contrast, the high La/Nb samples from Kurdistan show marked differences between the normalised values of the LILE (e.g. Ba/Rb, Th/K; Fig. 3a). Therefore rutile is a plausible control on the patterns of Nb and Ta, with the high La/Nb samples reflecting melting of the source where rutile is present in the residue. But, another phase or phases is/are needed to explain other trace element variations within the sample set.

A phlogopite-bearing source should be associated with higher K_2O values than are observed (Späth *et al.*, 2001), and Nb is highly incompatible with phlogopite (D_{Nb} <<1), so residual phlogopite is incapable of generating high La/Nb ratios (LaTourrette *et al.*, 1995; Green *et al.*, 2000). Carbonated mantle sources are thought to be associated with high Nb-Ta in derived melts (e.g. Hoernle *et al.*, 2002), and low Zr-Hf-Ti; this is not the overall signature of the Kurdistan lavas.

Amphibole may play a role in the chemical signatures, and the presence of amphibole in the source region has implications for the cause of melting discussed in the next section. High Ba/Rb ratios (Fig. 9) are consistent with K-richterite in the source, as $D_{Rb/Ba} > 1$ (Tiepolo *et al.*, 2003). Pargasite and kaersutite have $D_{Rb/Ba} < 1$, so are unlikely to control the high Ba/Rb seen in Fig. 9. K-richterite in the source also fits the relatively high K_2O values of ~3% (Späth *et al.*, 2001), and the negative Sr anomalies seen in the high La/Nb Qorveh-Bijar samples (Fig. 3; Tiepolo *et al.* 2003). However, this amphibole has D_{Nb} and D_{Ta} <<1 (Tiepolo *et al.*, 2003), and so could not be the cause of the variation seen in Nb and Ta.

It is not clear whether the key accessory minerals are distributed within the source area as distinct veins, more disseminated, or even as tectonically-emplaced slices of metasedimentary rock: the lack of reported xenoliths from the Kurdistan area hampers this evaluation. Typically, garnet peridotite does not contain accessory minerals such as rutile (Ionov and Hofmann, 1995), making it more plausible that other rock types within the source region contribute to the distinctive trace element signatures.

Metasomatic flux during Mesozoic-Cenozoic Tethyan subduction under Eurasia seems highly plausible as the process responsible for imparting the trace element signature of the Kurdistan lavas. The regional lithosphere was largely

assembled and accreted during the late Precambrian Pan-African orogeny, which could also have imparted an arc/subduction signature. However, Cenozoic alkaline lavas from the Arabian side of the Zagros suture lack such a signature (e.g. Lustrino *et al*., 2010), even though the regional basement is similar to the basement of Kurdistan Province.

In summary, the compositional spectrum of the Qorveh-Bijar lavas may be produced during melting of a source which becomes progressively depleted in garnet, amphibole, rutile and incompatible trace elements as partial melting proceeds, to generate the lowest La/Nb and La/Yb lavas.

Based on the combined elemental and isotopic data and modelling presented above, we propose a petrogenetic model for the Kurdistan lavas. Tethyan subduction under Eurasia would have fluxed subduction-derived fluids through the mantle lithosphere, enriching it in LILE, and imparting a negative Nb-Ta anomaly. Amphibole, rutile and, locally, phlogopite would have been stabilised in the mantle source, although the degree of metasomatism would have potentially been greater north and northeast of the study area, in the Urumieh-Dokhtar Magmatic Arc and its broad back-arc area (Fig. 1c; Vincent *et al.*, 2005; Moayyed *et al.,* 2008; Ahmadzadeh *et al.* 2010).

The intra-suite variations in La/Nb, Nb/Ta and Ba/Rb could happen either by progressively exhausting amphibole and rutile in the source region during melting, or melting shifting to a zone that originally lacked amphibole and rutile, but still lay within the garnet stability field. Both processes are variants of the same theme, that the Qorveh-Bijar volcanics show a progressive transition from trace element characteristics associated within subduction, towards patterns typically associated with within-plate magmatism. The key control is the presence or absence of

amphibole and rutile in the source region. Our preferred model is variation in the mineralogy during melting, as this appears simpler than having a source which is systematically variable in critical ratios and abundances on very small spatial and temporal scales (remembering that the sampled lavas were erupted within ~1 Myr across an area of only a few km^2).

The wider implication of this geochemical variation is that the subduction signature in continental magmatism can depend on the mineralogy of the source region, as well as the overall subduction flux derived from a previous or active subduction zone under the source area, given the right circumstances. We envisage that, in circumstances where the degree of melting is low, relatively small proportions of amphibole and/or rutile in the mantle source can be progressively exhausted during partial melting. Melt extraction would need to be a rapid process such that homogenisation of the melts does not occur. Thus a range of basaltic products can be generated, from rocks with large negative Nb-Ta anomalies and intra-LILE variation on normalised plots when amphibole and rutile are residual phases, to smaller Nb-Ta and LILE anomalies, reflecting the inherited subduction-related component, when amphibole and rutile are depleted.

This scenario is different to models for high Nb magmatism in convergent settings that appeal to tapping of an enriched source in the upper asthenosphere (e.g. Castillo *et al.*, 2002; Macpherson *et al.*, 2010), or partial melting of a mantle wedge in which significant quantities of amphibole had been precipitated during slab-melt-derived metasomatism (e.g. Kepezhinskas *et al.*, 1996; Hastie *et al.*, 2011). An amphibole component in peridotite is increasingly being invoked to explain the chemistry of volcanic suites from different tectonic settings (e.g. Class and Goldstein, 1997; Barry *et al.*, 2003; Pilet *et al.*, 2008; Chang *et al.*, 2009; Ma *et al.*, 2011), but it

is notable how variable these rocks are in their compositions, consistent with published composition, stability and partition coefficient data varying widely across the amphibole family of minerals.

Cause of melting

Two of the most popular models for generating magmatism in the Arabia-Eurasia collision zone are lithospheric delamination (e.g. Pearce *et al.*, 1990; Liotard *et al.*, 2008) and slab break-off (Keskin, 2003). Based on the thick lithosphere under the study area (~150-200 km; Priestley and McKenzie, 2006), these are both unlikely mechanisms for generating the Kurdistan lavas, although they are feasible for the large volcanic centres in eastern Turkey, Armenia and northwest Iran, where lithosphere thicknesses are low (~60 km; Angus *et al.* 2006).

There has been no regional late Cenozoic extension across the Turkish-Iranian plateau, or indeed localised extension in Kurdistan Province. This rules out the late stage orogenic extension mechanisms, appealed to in many centres further west around the Mediterranean (e.g. Prelević *et al.* 2008; Tommasini *et al.* 2011). Localised extension has been implicated elsewhere in Iran, especially along strike-slip systems (Walker *et al.,* 2009; Shabanian *et al.,* 2012). The northwest-southeast alignment of the volcanic centres in Kurdistan (Fig. 1d) is parallel to the main regional tectonic fabric, e.g. the Zagros suture itself (Fig. 1c), which implies at least some structural control on the final distribution of lavas. As active, orogen-parallel, northwest-southeast strike-slip shear occurs along the Zagros suture (Talebian and Jackson, 2002), it is possible that such shear has been involved in the transport of the magma through the crust of Kurdistan Province, but there is no evidence of it at exposed levels.

It is clear from the seismicity, GPS-derived velocity field and geomorphology that upper crustal shortening is not active (Vernant *et al.* 2004; Nissen *et al.* 2011; Allen *et al.* 2011a), and has not affected either the studied lavas or the Pliocene-Quaternary fluvial/lacustrine sediments that they overlie. This switch from compressional tectonics to a high plateau may well have triggered the melting and assisted its passage to the surface.

Shear heating has been suggested as a mechanism for generating small degree partial melts in mantle lithosphere (Kincaid and Silver, 1996), and the peak temperatures achieved (1050^{o}C at >90 km depth) lie close to the solidus of metasomatised peridotite at 1.8-2.5 GPa (Wallace and Green, 1991) but, as noted above, it is not clear from the surface geology in Kurdistan that there is Quaternary shear at depth, making this a highly speculative mechanism regardless of more general problems associated with the process, such as the ability to keep generating heat once viscosity has been lowered, upon reaching the mantle lithosphere (Kameyama *et al.*, 1999).

An important aspect of the regional geological history is that the Eurasian plate lithosphere would have been affected by Tethyan oceanic subduction and later underthrusting of the Arabian margin during collision. Fluxes derived from the downgoing plate could impart a subduction-related trace element signature to the future Eurasian plate source region. A hydrated, metasomatised source region would have a lower solidus than either anhydrous peridotite or peridotite disseminated with small amounts of amphibole.

Furthermore, such fertile, metasomatised peridotite might cross its solidus during lithospheric *thickening*, as a result of the convergent tectonics of the collision zone. This model is based on the looped shape of the amphibole solidus with its

section of negative slope dT/dP (the "backbend" of Green, 1973; Green and Falloon, 2005; Fig. 12). The shape of the solidus implies that a weakly hydrated amphibole peridotite (~1000-1100ºC, 0.2% H_2O) at a starting depth of ~90 km will partially melt during further burial.

Green (1973) has shown experimentally that basanite or alkali basalt magma would be the product of such melting. The loop on the pargasitic amphibole peridotite solidus straightens out at higher H_2O content (6% in the model of Green, 1973), which implies that a truly wet peridotite source, perhaps influenced by a very large recent fluid flux from a down-going oceanic slab, would not produce melt via further burial. Nevertheless, such compressional melting has previously been associated with down-flow of asthenospheric mantle during convection in the mantle wedge above a subduction zone (Iwamori, 1997), but lithospheric thickening and burial achieves an equivalent pressure-temperature pathway.

One caveat is that the temperature of the lithosphere must be high enough at appropriate depths (and this is an issue for all possible melting models, given the reported thick lithosphere of the region). It may be that the geotherm has a backbend because of underthrusting of the Arabian passive margin under the Eurasian active margin during the collision: simple, near-linear geotherms more typical of stable areas such as cratons (Mather *et al.*, 2011), are unlikely to apply in active orogenic belts. Maggi and Priestley (2005) reported low shear wave velocities zone at ~100 km depth under the Turkish-Iranian plateau, which they interpreted as indicating anomalously warm, low density upper mantle beneath the region, consistent with a low degree of partial melting.

Many examples of collision zone magmatism have been interpreted as the result of melting of mantle metasomatised during previous subduction (e.g. Prelević *et*

al. 2008; Tommasini *et al.* 2011), and the Kurdistan lavas potentially have a similar kind of source, given the Tethyan subduction under the Iranian (Eurasian) margin before collision.

It is notable that the lower La/Nb samples, modelled as the result of higher degrees of melting, occur later than the more extensive flows - perhaps when amphibole is nearly exhausted in the source region. Once amphibole is exhausted, this melting mechanism is no longer viable, and magmatism rapidly wanes (Fig. 12).

To our knowledge, this compression-melting mechanism has not previously been implicated in the origin of mafic magmatism in continental collision settings. It may be relevant to lavas in northern Tibet that were generated in the garnet stability field (e.g. Zhang *et al.*, 2008): these are conventionally explained as triggered by asthenospheric upwelling, perhaps following lithosphere delamination. The Tibetan lithosphere thickness estimates of Priestley and McKenzie (2006) are ≥200 km, which cast doubt on the viability of the delamination model for these rocks. Compression-related melting fits the chemical and tectonic constraints.

Comparison with regional late Cenozoic magmatism

The volcanic rocks from Kurdistan are one small part of the late Cenozoic magmatism generated within the Arabia-Eurasia collision zone, as noted in section 2. Different lavas in this study possess affinities with the Ararat and Tendürek composite volcanoes on the Iran/Turkey borderlands (Kheirkhah *et al.*, 2009; TBQ5.4), potassic lavas from NW Iran (Ahmadzadeh *et al.*, 2010; the two flows from Takab) or Damavand (Davidson *et al.*, 2004; majority of the Qorveh-Bijar samples). A notable feature of basaltic lavas from Damavand is that they show the same range of La, Nb and La/Nb as the Qorveh-Bijar samples (Fig. 4; Davidson *et al.*, 2004; Liotard *et al.*,

2008; Mirnejad *et al.*, 2010; Davidson, unpublished data), hinting that a similar source is present, and that an equivalent melting regime may operate under both regions to generate their matching compositions.

A safe conclusion to be drawn is that the mantle within the Arabia-Eurasia collision zone is very heterogeneous in structure and composition, and capable of melting under a variety of PT conditions to produce the observed range of chemistries. The Kurdistan lavas show how much of the collision-wide compositional range can be found within an area ~100 km across, suggesting rapid variation within the mantle lithosphere and/or melting conditions.

Verdel *et al.* (2011) have recently documented how Oligocene volcanics across Iran possess smoother spidergrams than their more extensive Eocene counterparts, which they related to greater asthenospheric input and waning hydration of the source. We speculate that the source region was essentially the same between the Eocene and Oligocene, but the main control on the changing chemistry was the reduction or exhaustion in amphibole and rutile in the mantle source, following the end of Neo-Tethyan subduction.

Eastern China and adjacent areas provide another potential application of the ideas in this study: extensive Mesozoic/early Cenozoic arc and back-arc magmatism was followed by late Cenozoic basic volcanics with within-plate chemistries (e.g. low La/Nb, alkalic), but lithospheric isotopic signatures (e.g. Zou *et al.*, 2000). Possibly, there was an exhaustion of amphibole and rutile in the mantle sources over time, contributing to the transfer from arc to within-plate chemical signatures.

CONCLUSIONS

Quaternary lavas from Kurdistan Province, Iran, are typically small degree melts generated in the garnet stability field from thick lithosphere of the Turkish-Iranian plateau. Sodic basanites, hawaiites and alkali basalts from Qorveh and Bijar show a range of trace element signatures, from spiky spidergrams reminiscent of subduction-modified magmatism, to smooth LILE and HFSE traces that resemble OIB, although always having some subduction signature (e.g. La/Nb >1). Both types occur within the same volcanic centre within 1 Myr, and only show minor variation in Sr-Nd isotopic values, with no clear correlation between the Sr-Nd isotopic composition and trace element signatures. The higher La/Nb, subduction-signature rocks typically possess higher La/Yb, indicating smaller degrees of melting, and/or a more fertile source.

We do not believe this compositional range represents crustal contamination, fractionation, or the chance juxtaposition of fundamentally different mantle source regions. The ratios of REE can be modelled by melting of a garnet-amphibole peridotite. Varying amounts of amphibole (likely K-richterite) in the source are likely to control intra-LILE variation, with rutile controlling Nb and Ta abundances and hence the threefold variation in La/Nb.

Compositions are consistent with a flux of incompatible elements into the Eurasian mantle lithosphere during pre-collision Neo-Tethyan subduction, and early stages of continental collision, with Quaternary melting following initial collision by as much as 35 Ma. The importance of this result is that the later production of subduction or within-plate characteristics during continental lithosphere melting need not reflect wholesale changing of mantle source(s), but can result from mineralogical control, specifically the abundance of amphibole and rutile in the source. Other magmatic provinces with changes from arc to within-plate characteristics may share

this control, e.g. the Palaeogene magmatism of Iran and the Mesozoic-Cenozoic magmatism of eastern China.

Flows from near Takab in the north of the study area are potassic, and have high Rb/Sr and low Ba/Rb, consistent with a component of phlogopite in the source.

The precise mechanism for generating the Kurdistan lavas is unclear, but the thick lithosphere of the collision zone (up to ~200 km) makes lower lithosphere delamination or slab break-off unlikely. An intriguing possibility is that the inferred amphibole-bearing source began to melt as the result of lithosphere thickening, crossing the amphibole peridotite solidus with a downward trajectory (Fig. 12). This melt mechanism may be applicable to other orogenic plateau magmatism, including late Cenozoic volcanic rocks of northern Tibet.

FUNDING

This work was supported by the Natural Environment Research Council [grant number NE/H021620/1 “Orogenic plateau magmatism”].

ACKNOWLEDGEMENTS

We thank Nick Marsh, Chris Ottley and Geoff Nowell for help with sample analyses. The Director and staff of the Geological Survey of Iran are thanked for their scientific and logistical support. Jon Davidson, Colin Macpherson, Helen Williams and Simone Tommasini provided useful discussion. MK and MBA also thank the Royal Society for travel grants. We thank Stephen Foley, Massimo Tiepolo and an anonymous referee for their very helpful reviews.

REFERENCES

Aftabi, A. & Atapour, H. (2000). Regional aspects of shoshonitic volcanism in Iran. *Episodes* **23**, 119-125.

Agard, P., Omrani, J., Jolivet, L. & Mouthereau, F. (2005). Convergence history across Zagros (Iran): constraints from collisional and earlier deformation. *International Journal of Earth Sciences* **94**, 401-419.

Agard, P., Omrani, J., Jolivet, L., Whitechurch, H., Vrielynck, B., Spakman, W., Monie, P., Meyer, B. & Wortel, R. (2011). Zagros orogeny: a subduction-dominated process. *Geological Magazine*, **148**, 692-725.

Ahmadzadeh, G., Jahangiri, A., Lentz, D. & Mojtahedi, M. (2010). Petrogenesis of Plio-Quaternary post-collisional ultrapotassic volcanism in NW of Marand, NW Iran. *Journal of Asian Earth Sciences* **39**, 37-50.

Allen, M., Jackson, J. & Walker, R. (2004). Late Cenozoic reorganization of the Arabia-Eurasia collision and the comparison of short-term and long-term deformation rates. *Tectonics* **23**, TC2008, doi: 2010.1029/2003TC001530.

Allen, M. B. & Armstrong, H. A. (2008). Arabia-Eurasia collision and the forcing of mid Cenozoic global cooling. *Palaeogeography Palaeoclimatology Palaeoecology* **265**, 52-58.

Allen, M. B., Kheirkhah, M., Emami, M. H. & Jones, S. J. (2011a). Right-lateral shear across Iran and kinematic change in the Arabia-Eurasia collision zone. *Geophysical Journal International* **184**, 555-574.

Allen, M. B., Mark, D. F., Kheirkhah, M., Barfod, D., Emami, M. H. & Saville, C. (2011b). $^{40}Ar/^{39}Ar$ dating of Quaternary lavas in northwest Iran: constraints on the landscape evolution and incision rates of the Turkish-Iranian plateau. *Geophysical Journal International* **185**, 1175-1188.

Angus, D. A., Wilson, D. C., Sandvol, E. & Ni, J. F. (2006). Lithospheric structure of the Arabian and Eurasian collision zone in eastern Turkey from S-wave receiver functions. *Geophysical Journal International* **166**, 1335-1346.

Ballato, P., Uba, C. E., Landgraf, A., Strecker, M. R., Sudo, M., Stockli, D. F., Friedrich, A. & Tabatabaei, S. H. (2011). Arabia-Eurasia continental collision: Insights from late Tertiary foreland-basin evolution in the Alborz Mountains, northern Iran. *Geological Society of America Bulletin* **123**, 106-131.

Barry, T. L., Saunders, A. D., Kempton, P. D., Windley, B. F., Pringle, M. S., Dorjnamjaa, D. & Saandar, S. (2003). Petrogenesis of Cenozoic basalts from Mongolia: Evidence for the role of asthenospheric versus metasomatized lithospheric mantle sources. *Journal of Petrology* **44**, 55-91.

Berberian, F., Muir, I. D., Pankhurst, R. J. & Berberian, M. (1982). Late Cretaceous and early Miocene Andean-type plutonic activity in northern Makran and Central Iran. *Journal of the Geological Society* **139**, 605-614.

Berberian, M. & King, G. C. P. (1981). Towards a paleogeography and tectonic evolution of Iran. *Canadian Journal of Earth Sciences* **18**, 210-265.

Berberian, M. & Yeats, R. S. (1999). Patterns of historical earthquake rupture in the Iranian plateau. *Bulletin of the Seismological Society of America* **89**, 120-139.

Boccaletti, M., Innocenti, F., Manetti, P., Mazzuoli, R., Motamed, A., Pasquare, G., Radicati di Brozolo, F. & Amin Sobhani, E. (1976). Neogene and quaternary volcanism of the Bijar Area (Western Iran). *Bulletin of Volcanology* **40**, 122-132.

Bridgland, D. R., Demir, T., Seyrek, A., Pringle, M., Westaway, R., Bieck, A. R., Rowbotham, G. & Yurtmeni, S. (2007). Dating quaternary volcanism and incision by the river Tigris at Diyarbakir, southeast Turkey. *Journal of Quaternary Science* **22**, 387-393.

Buket, E. & Temel, A. (1998). Major-element, trace-element, and Sr-Nd isotopic geochemistry and genesis of Varto (Mus) volcanic rocks, eastern Turkey. *Journal of Volcanology and Geothermal Research* **85**, 405-422.

Castillo, P. R., Solidum, R. U. & Punongbayan, R. S. (2002). Origin of high field strength element enrichment in the Sulu Arc, southern Philippines, revisited. *Geology* **30**, 707-710.

Chang, J. M., Feeley, T. C. & Deraps, M. R. (2009). Petrogenesis of basaltic volcanic rocks from the Pribilof Islands, Alaska, by melting of metasomatically enriched depleted lithosphere, crystallization differentiation, and magma mixing. *Journal of Petrology* **50**, 2249-2286.

Choi, S. H., Mukasa, S. B., Andronikov, A. V. & Marcano, M. C. (2007). Extreme Sr–Nd–Pb–Hf isotopic compositions exhibited by the Tinaquillo peridotite massif, Northern Venezuela: implications for geodynamic setting. *Contributions to Mineralogy and Petrology* **153**, 443-463.

Class, C. & Goldstein, S. L. (1997). Plume-lithosphere interactions in the ocean basins: constraints from the source mineralogy. *Earth and Planetary Science Letters* **150**, 245-260.

Cox, K.G., Bell, J.D. & Pankhurst, R.J. (1979). *The classification of igneous rocks*. London: Allen and Unwin.

Daliran, F. (2008). The carbonate rock-hosted epithermal gold deposit of Agdarreh, Takab geothermal field, NW Iran - hydrothermal alteration and mineralisation. *Mineralium Deposita* **43**, 383-404.

Davidson, J., Hassanzadeh, J., Berzins, R., Stockli, D. F., Bashukooh, B., Turrin, B. & Pandamouz, A. (2004). The geology of Damavand volcano, Alborz Mountains, northern Iran. *Geological Society of America Bulletin* **116**, 16-29.

Davidson, J., Turner, S., Handley, H., Macpherson, C. & Dosseto, A. (2007). Amphibole "sponge" in arc crust? *Geology* **35**, 787-790.

Dewey, J. F. (1988). Extensional collapse of orogens. *Tectonics* **7**, 1123-1139.

Dilek, Y., Imamverdiyev, N. & Altunkaynak, S. (2010). Geochemistry and tectonics of Cenozoic volcanism in the Lesser Caucasus (Azerbaijan) and the peri-Arabian region: collision-induced mantle dynamics and its magmatic fingerprint. *International Geology Review* **52**, 536-578.

Dowall, D. P., Nowell, G. M. & Pearson, D. G. (2003). Chemical pre-concentration procedures for high-precision analysis of Hf-Nd-Sr isotopes in geological materials by plasma ionisation multi-collector mass spectrometry (PIMMS) techniques. I. In: Holland, J. G. & Tanner, S. D. (eds.) *Plasma Source Mass Spectrometry: Applications and Emerging Technologies.* Cambridge: The Royal Society of Chemistry, 321-337.

Emami, M. H., Sadeghi, M. M. M. & Omrani, S. J. (1993). Magmatic map of Iran. Tehran: Geological Survey of Iran.

Foley, S. (2008). A trace element perspective on Archean crust formation and the presence or absence of Archean subduction. In: Condie, K. C. & Pease, V. (eds.) *When Did Plate Tectonics Begin on Planet Earth?* Geological Society of America, Special Paper **440**, 31-50.

Foley, S., Tiepolo, M. & Vannucci, R. (2002). Growth of early continental crust controlled by melting of amphibolite in subduction zones. *Nature* **417**, 837-840.

Foley, S. F., Barth, M. G. & Jenner, G. A. (2000). Rutile/melt partition coefficients for trace elements and an assessment of the influence of rutile on the trace element characteristics of subduction zone magmas. *Geochimica Et Cosmochimica Acta* **64**, 933-938.

Foley, S. F. & Wheller, G. E. (1990). Parallels in the origin of the geochemical signatures of island-arc volcanics and continental potassic igneous rocks - the role of residual titanates. *Chemical Geology* **85**, 1-18.

Fréménias, O., Coussaert, N., Berger, J., Mercier, J-C. C. & Demaiffe, D. (2004). Metasomatism and melting history of a Variscan lithospheric mantle domain: evidence from the Puy Beaunit xenoliths (French Massif Central). *Contributions to Mineralogy and Petrology* **148**, 13-28.

Frizon de Lamotte, D., Raulin, C., Mouchot, N., Wrobel-Daveau, J. C., Blanpied, C. & Ringenbach, J. C. (2011). The southernmost margin of the Tethys realm during the Mesozoic and Cenozoic: Initial geometry and timing of the inversion processes. *Tectonics* **30**, Tc3002 doi: 10.1029/2010tc002691.

Furman, T. & Graham, D. (1999). Erosion of lithospheric mantle beneath the East African Rift system: geochemical evidence from the Kivu volcanic province. *Lithos* **48**, 237-262.

Green, D. H. (1973). Experimental melting studies on a model upper mantle composition at high-pressure under water-saturated and water-undersaturated conditions. *Earth and Planetary Science Letters* **19**, 37-53.

Green, D. H. & Falloon, T. J. (2005). Primary magmas at mid-ocean ridges, "hotspots," and other intraplate settings: Constraints on mantle potential temperature. In: Foulger, G. R., Natland, J. H., Presnall, D. C. & Anderson, D. L. (eds.) *Plates, Plumes and Paradigms*: Geological Society of America, 217-248.

Green, T. H., Blundy, J. D., Adam, J. & Yaxley, G. M. (2000). SIMS determination of trace element partition coefficients between garnet, clinopyroxene and hydrous basaltic liquids at 2-7.5 GPa and 1080-1200 degrees C. *Lithos* **53**, 165-187.

Guo, Z. F., Wilson, M., Liu, J. Q. & Mao, Q. (2006). Post-collisional, potassic and ultrapotassic magmatism of the northern Tibetan Plateau: Constraints on characteristics of the mantle source, geodynamic setting and uplift mechanisms. *Journal of Petrology* **47**, 1177-1220.

Hart, S.R. (1988). Heterogeneous mantle domains: signatures, genesis and mixing chronologies. *Earth and Planetary Science Letters* **90**, 273-296.

Hastie, A. R., Mitchell, S. F., Kerr, A. C., Minifie, M. J. & Millar, I. L. (2011). Geochemistry of rare high-Nb basalt lavas: Are they derived from a mantle wedge metasomatised by slab melts? *Geochemica et Cosmochemica Acta* **75**, 5049-5072.

Hoernle, K., Tilton, G., Le Bas, M. J., Duggan, S. & Garde-Schonberg, D. (2002). Geochemistry of oceanic carbonatites compared with continental carbonatites: mantle recycling of oceanic crustal carbonate. *Contribution to Mineralogy and Petrology,* **142**, 520-542.

Ionov, D. A. & Hofmann, A. W. (1995). Nb-Ta-rich mantle amphiboles and micas - implications for subduction-related metasomatic trace-element fractionations. *Earth and Planetary Science Letters* **131**, 341-356.

Iwamori, H. (1997). Compression melting in subduction zones. *Terra Nova* **9**, 9-13.Jackson, J., Haines, A. J. & Holt, W. E. (1995). The accommodation of Arabia-Eurasia plate convergence in Iran. *Journal of Geophysical Research* **100**, 15205-15209.

Jahangiri, A. (2007). Post-collisional Miocene adakitic volcanism in NW Iran: Geochemical and geodynamic implications. *Journal of Asian Earth Sciences* **30**, 433-447.

Kameyama, M., Yuen, D. A. & Karato, S. I. (1999). Thermal-mechanical effects of low-temperature plasticity (the Peierls mechanism) on the deformation of a viscoelastic shear zone. *Earth and Planetary Science Letters* **168**, 159-172.

Kazmin, V. G., Sborshchikov, I. M., Ricou, L.-E., Zonenshain, L. P., Boulin, J. & Knipper, A. L. (1986). Volcanic belts as markers of the Mesozoic-Cenozoic active margin of Eurasia. *Tectonophysics* **123**, 123-152.

Kelemen, P. B., Shimizu, N. & Dunn, T. (1993). Relative depletion of niobium in some arc magmas and the continental crust - partitioning of K, Nb, La and Ce during melt/rock reaction in the upper mantle. *Earth and Planetary Science Letters* **120**, 111-134.

Kepezhinskas, P., Defant, M. J. & Drummond, M. S. (1996). Progressive enrichment of island arc mantle by melt-peridotite interaction inferred from Kamchatka xenoliths. *Geochimica Et Cosmochimica Acta* **60**, 1217-1229.

Keskin, M. (2003). Magma generation by slab steepening and breakoff beneath a subduction-accretion complex: An alternative model for collision-related volcanism in Eastern Anatolia, Turkey. *Geophysical Research Letters* **30**, 1-4.

Keskin, M. (2007). Eastern Anatolia: a hot spot in a collision zone without a mantle plume. In: Foulger, G. R. & Jurdy, D. M. (eds.) *Plates, Plumes, and Planetary Processes*: Geological Society of America, Special Paper **409**, 1-25.

Keskin, M., Pearce, J. A. & Mitchell, J. G. (1998). Volcano-stratigraphy and geochemistry of collision-related volcanism on the Erzurum-Kars Plateau, northeastern Turkey. *Journal of Volcanology and Geothermal Research* **85**, 355-404.

Kheirkhah, M., Allen, M. B. & Emami, M. (2009). Quaternary syn-collision magmatism from the Iran/Turkey borderlands. *Journal of Volcanology and Geothermal Research* **182**, 1-12.

Kincaid, C. & Silver, P. (1996). The role of viscous dissipation in the orogenic process. *Earth and Planetary Science Letters* **142**, 271-288.

Kirchenbaur, M., Münker, C., Schuth, S., Garbe-Schönberg, D. & Marchev, P. (2012). Tectonomagmatic constraints on the sources of eastern Mediterranean K-rich lavas. *Journal of Petrology* **53**, 27-65.

Klein, M., Stosch, H. G. & Seck, H. A. (1997). Partitioning of high field-strength and rare-earth elements between amphibole and quartz-dioritic to tonalitic melts: An experimental study. *Chemical Geology* **138**, 257-271.

Latourrette, T., Hervig, R. L. & Holloway, J. R. (1995). trace-element partitioning between amphibole, phlogopite, and basanite melt. *Earth and Planetary Science Letters* **135**, 13-30.

Liotard, J. M., Dautria, J. M., Bosch, D., Condomines, M., Mehdizadeh, H. & Ritz, J. F. (2008). Origin of the absarokite-banakite association of the Damavand volcano (Iran): trace elements and Sr, Nd, Pb isotope constraints. *International Journal of Earth Sciences* **97**, 89-102.

Lustrino, M., Keskin, M., Mattioli, M., Lebedev, V. A., Chugaev, A., Sharkov, E. & Kavak, O. (2010). Early activity of the largest Cenozoic shield volcano in the circum-Mediterranean area: Mt. Karacadag, SE Turkey. *European Journal of Mineralogy* **22**, 343-362.

Ma, G. S. K., Malpas, J., Xenophontos, C. & Chan, G. H. N. (2011). Petrogenesis of Latest Miocene-Quaternary Continental Intraplate Volcanism along the Northern Dead Sea Fault System (Al Ghab-Homs Volcanic Field), Western Syria: Evidence for Lithosphere-Asthenosphere Interaction. *Journal of Petrology* **52**, 401-430.

Macpherson, C. G., Chiang, K. K., Hall, R., Nowell, G. M., Castillo, P. R. & Thirlwall, M. F. (2010). Plio-Pleistocene intra-plate magmatism from the southern Sulu Arc, Semporna peninsula, Sabah, Borneo: Implications for high-Nb basalt in subduction zones. *Journal of Volcanology and Geothermal Research* **190**, 25-38.

Maggi, A. & Priestley, K. (2005). Surface waveform tomography of the Turkish-Iranian plateau. *Geophysical Journal International* **160**, 1068-1080.

Mather, K. A., Pearson, D. G., McKenzie, D., Kjarsgaard, B. A. & Priestley, K. (2011). Constraints on the depth and thermal history of cratonic lithosphere from peridotite xenoliths, xenocrysts and seismology *Lithos* **125**, 729-742.

McQuarrie, N., Stock, J. M., Verdel, C. & Wernicke, B. (2003). Cenozoic evolution of Neotethys and implications for the causes of plate motions. *Geophysical Research Letters* **30**, art. no. 2036 doi 2010.1029/2003GL017992.

Mirnejad, H., Hassanzadeh, J. Cousens, B. L. & Taylor, B. E. (2010). Geochemical evidence for deep mantle melting and lithospheric delamination as the origin of the inland Damavand volcanic rocks of northern Iran. *Journal of Volcanology and Geothermal Research* **198**, 288-296.

Moayyed, M., Moazzen, M., Calagari, A. A., Jahangiri, A. & Modjarrad, M. (2008). Geochemistry and petrogenesis of lamprophyric dykes and the associated rocks from Eslamy peninsula, NW Iran: Implications for deep-mantle metasomatism. *Chemie Der Erde-Geochemistry* **68**, 141-154.

Morley, C. K., Kongwung, B., Julapour, A. A., Abdolghafourian, M., Hajian, M., Waples, D., Warren, J., Otterdoom, H., Srisuriyon, K. & Kazemi, H. (2009). Structural development of a major late Cenozoic basin and transpressional belt in central Iran: The Central Basin in the Qom-Saveh area. *Geosphere* **5**, 325-362.

Mouthereau, F. (2011). Timing of uplift in the Zagros belt/Iranian plateau and accommodation of late Cenozoic Arabia–Eurasia convergence. *Geological Magazine* **148**, 726-738.

Münker, C., Pfänder, J. A., Weyer, S., Buchl, A., Kleine, T. & Mezger, K. (2003). Evolution of planetary cores and the earth-moon system from Nb/Ta systematics. *Science* **301**, 84-87.

National Iranian Oil Company. (1978). Geological Map of Iran Sheet 1 North-West Iran. Tehran: National Iranian Oil Company.

Nissen, E., Tatar, M., Jackson, J. A. & Allen, M. B. (2011). New views on earthquake faulting in the Zagros fold-and-thrust belt of Iran. *Geophyical Journal International* **186**, 928-944.

Notsu, K., Fujitani, T., Ui, T., Matsuda, J. & Ercan, T. (1995). Geochemical features of collision-related volcanic-rocks in central and eastern Anatolia, Turkey. *Journal of Volcanology and Geothermal Research* **64**, 171-191.

Nowell, G. M., Pearson, D. G., Ottley, C. J., Schweiters, J. & Dowall, D. (2003). Long-term performance characteristics of a plasma ionisation multi-collector mass spectrometer (PIMMS): the ThernoFinnigan Neptune. In: Holland, J. G. & Tanner, S. D. (eds.) *Plasma Source Mass Spectrometry: Applications and Emerging Technologies*. Cambridge: The Royal Society of Chemistry, 307-320.

Okay, A. I., Zattin, M. & Cavazza, W. (2010). Apatite fission-track data for the Miocene Arabia-Eurasia collision. *Geology* **38**, 35-38.

Omrani, J., Agard, P., Whitechurch, H., Benoit, M., Prouteau, G. & Jolivet, L. (2008). Arc-magmatism and subduction history beneath the Zagros Mountains, Iran: A new report of adakites and geodynamic consequences. *Lithos* **106**, 380-398.

Orejana, D., Villaseca, C. & Paterson, B. A. (2006). Geochemistry of pyroxenitic and hornblenditic xenoliths in alkaline lamprophyres from the Spanish Central System. *Lithos* **86**, 167-196.

Ottley, C. J., Pearson, D. G. & Irvine, G. J. (2003). A routine method for the dissolution of geological samples for the analysis of REE and trace elements via ICP-MS. In: Holland, J. G. & Tanner, S. D. (eds.) *Plasma Source Mass Spectrometry: Applications and Emerging Technologies*. Cambridge: Royal Society of Chemistry, 221-230.

Özdemir, Y., Karaoğlu, O., Tolluoğlu, A. O. & Güleç, N. (2006). Volcano stratigraphy and petrogenesis of the Nemrut stratovolcano (East Anatolian High Plateau): The most recent post-collisional volcanism in Turkey. *Chemical Geology* **226**, 189-211.

Parlak, O., Delaloye, M., Demirkol, C. & Unlugenc, U. C. (2001). Geochemistry of Pliocene/Pleistocene basalts along the Central Anatolian Fault Zone (CAFZ), Turkey. *Geodinamica Acta* **14**, 159-167.

Paul, A., Hatzfeld, D., Kaviani, A., Tatar, M. & Péquegnat, C. (2010). Seismic imaging of the lithospheric structure of the Zagros mountain belt (Iran). In: Leturmy, P. & Robin, C. (eds.) *Tectonic and Stratigraphic Evolution of Zagros and Makran during the Mesozoic–Cenozoic*: Geological Society, London, Special Publications, 5-18.

Pearce, J. A., Bender, J. F., Delong, S. E., Kidd, W. S. F., Low, P. J., Guner, Y., Sargolu, F., Yilmaz, Y., Moorbath, S. & Mitchell, J. G. (1990). Genesis of collision volcanism in eastern Anatolia, Turkey. *Journal of Volcanology and Geothermal Research* **44**, 189-229.

Pearce, J. A. & Peate, D. W. (1995). Tectonic implications of the composition of volcanic arc magmas. *Annual Review of Earth and Planetary Sciences* **23**, 251-285.

Pfänder, J. A., Münker, C., Stracke, A. & Mezger, K. (2007). Nb/Ta and Zr/Hf in ocean island basalts - Implications for crust-mantle differentiation and the fate of Niobium. *Earth and Planetary Science Letters* **254**, 158-172.

Pilet, S., Baker, M. B. & Stolper, E. M. (2008). Metasomatized lithosphere and the origin of alkaline lavas. *Science* **320**, 916-919.

Plank, T. & Langmiur, C. H. (1998). The chemical composition of subducting sediment and its consequences for the crust and mantle. *Chemical Geology* **145**, 325-394.

Prelević, D., Foley, S. F., Romer, R. & Conticelli, S. (2008). Mediterranean Tertiary lamproites derived from multiple source components in postcollisional dynamics. *Geochemica et Cosmochemica Acta* **72**, 2125-2156.

Priestley, K. & McKenzie, D. (2006). The thermal structure of the lithosphere from shear wave velocities. *Earth and Planetary Science Letters* **244**, 285-301.

Reagan, M. K. & Gill, J. B. (1989). Co-existing calc-alkaline and high-Niobium basalts from Turrialba volcanco, Coata-Rica - implications for residual titanates in arc magma sources. *Journal of Geophysical Research-Solid Earth and Planets* **94**, 4619-4633.

Rudnick, R. L. & Fountain, D. M. (1995). Nature and composition of the continental crust: A lower crustal perspective. *Reviews of Geophysics* **33**, 267-309.

Saadat, S. & Stern, C. R. (2011). Petrochemistry and genesis of olivine basalts from small monogenetic parasitic cones of Bazman stratovolcano, Makran arc, southeastern Iran. *Lithos* **125**, 607-619.

Schmidt, M. W., Dardon, A., Chazot, G. & Vannucci, R. (2004). The dependence of Nb and Ta rutile-melt partitioning on melt composition and Nb/Ta fractionation during subduction processes. *Earth and Planetary Science Letters* **226**, 415-432.

Sen, P. A., Temel, A. & Gourgaud, A. (2004). Petrogenetic modelling of Quaternary post-collisional volcanism: a case study of central and eastern Anatolia. *Geological Magazine* **141**, 81-98.

Şengör, A. M. C. (1986). The dual nature of the Alpine-Himalayan system: progress, problems and prospects. *Tectonophysics* **127**, 177-195.

Şengör, A. M. C., Altiner, D., Cin, A., Ustaomer, T. & Hsu, K. J. (1988). Origin and assembly of the Tethyside orogenic collage at the expense of Gondwana Land. In: Audley-Charles, M. G. & Hallam, A. (eds.) *Gondwana and Tethys*: Geological Society, London, 119-181.

Shabanian, E., Bellier, O., Siame, L., Arnaud, N., Abbassi, M. R. & Cocheme, J. J. (2009). New tectonic configuration in NE Iran: Active strike-slip faulting between the Kopeh Dagh and Binalud mountains. *Tectonics* **28**, Tc5002, doi: 10.1029/2008tc002444.

Shabanian, E., Acocella, V., Gioncada, A., Ghasemi, H. & Bellier, O. (2012). Structural control on volcanism in intraplate post collisional settings: Late Cenozoic to Quaternary examples of Iran and Eastern Turkey. *Tectonics* **31**, Tc3013, doi: 10.1029/2011TC003042.

Shaw, D. M. (1970). Trace element fractionation during anatexis. *Geochimica et Cosmochimica Acta* **34**, 237-247.

Späth, A., Le Roex, A. P. & Opiyo-Akech, N. (2001). Plume-lithosphere interaction and the origin of continental rift-related alkaline volcanism - the Chyulu Hills Volcanic Province, southern Kenya. *Journal of Petrology* **42**, 765-787.

Stampfli, G. M. & Borel, G. D. (2002). A plate tectonic model for the Paleozoic and Mesozoic constrained by dynamic plate boundaries and restored synthetic oceanic isochrons. *Earth and Planetary Science Letters* **196**, 17-33.

Sun, S. S. & McDonough, W. F. (1989). Chemical and isotopic systematics of oceanic basalts: implications for mantle composition and processes. In: Saunders, A. D. & Norry, M. J. (eds.) *Magmatism in the Ocean Basins*: Geological Society of London Special Publication, 313-345.

Talebian, M. & Jackson, J. (2002). Offset on the Main Recent Fault of NW Iran and implications for the late Cenozoic tectonics of the Arabia–Eurasia collision zone. *Geophysical Journal International* **150**, 422-439.

Tarney, J. & Marsh, N. G. (1991). Major and trace element geochemistry of Holes CY-1 and CY-4 : Implications for petrogenetic models. In: Gibson, I. L., Malpas, J., Robinson, P. A. & Xenophontos, C. (eds.) *Initial Reports, Holes CY-1and CY-1A*: Geological Survey of Canada, 133-175.

Thirlwall, M. F., Upton, B. G. J. & Jenkins, C. (1994). Interaction between continental lithoshere and the Iceland plume - Sr-Nd-Pb isotope geochemistry of Tertiary basalts, NE Greenland. *Journal of Petrology* **35**, 839-879.

Tiepolo, M., Vannucci, R., Oberti, R., Foley, S., Bottazzi, P. & Zanetti, A. (2000). Nb and Ta incorporation and fractionation in titanian pargasite and kaersutite: crystal-chemical constraints and implications for natural systems. *Earth and Planetary Science Letters* **176**, 185-201.

Tiepolo, M., Zanetti, A., Oberti, R., Brumm, R., Foley, S. & Vannucci, R. (2003). Trace-element partitioning between synthetic potassic-richterites and silicate melts, and contrasts with the partitioning behaviour of pargasites and kaersutites. *European Journal of Mineralogy* **15**, 329-340.

Tommasini, S., Avanzinelli, R. & Conticelli, S. (2011). The Th/La and Sm/La conundrum of the Thethyan realm lamproites. *Earth and Planetary Science Letters* **301**, 469-478.

van Hunen, J. & Allen, M. B. (2011). Continental collision and slab break-off: A comparison of 3-D numerical models with observations. *Earth and Planetary Science Letters* **302**, 27-37.

Verdel, C., Wernicke, B. P., Hassanzadeh, J. & Guest, B. (2011). A Paleogene extensional arc flare-up in Iran. *Tectonics* **30**.

Vernant, P., Nilforoushan, F., Hatzfeld, D., Abbassi, M., Vigny, C., Masson, F., Nankali, H., Martinod, J., Ashtiani, A., Bayer, R., Tavakoli, F. & Chery, J. (2004). Contemporary crustal deformation and plate kinematics in Middle East constrained by GPS measurements in Iran and northern Iran. *Geophysical Journal International* **157**, 381-398.

Vincent, S. J., Allen, M. B., Ismail-Zadeh, A. D., Flecker, R., Foland, K. A. & Simmons, M. D. (2005). Insights from the Talysh of Azerbaijan into the Paleogene evolution of the South Caspian region. *Bulletin of the Geological Society of America* **117**, 1513-1533.

Walker, R. T., Gans, P., Allen, M. B., Jackson, J., Khatib, M., Marsh, N. & Zarrinkoub, M. (2009). Late Cenozoic volcanism and rates of active faulting in eastern Iran. *Geophyical Journal International* **177**, 783-805.

Wallace, M. E. & Green, D. H. (1991). The effect of bulk rock composition on the stability of amphibole in the upper mantle - implications for solidus positions and mantle metasomatism. *Mineralogy and Petrology* **44**, 1-19.

Williams, H. M., Turner, S. P., Pearce, J. A., Kelley, S. P. & Harris, N. B. W. (2004). Nature of the source regions for post-collisional, potassic magmatism in southern and northern Tibet from geochemical variations and inverse trace element modelling. *Journal of Petrology* **45**, 555-607.

Wilson, M. (1989). *Igneous Petrogenesis*. London: Unwin Hyman.

Workman, R. K., & Hart, S. R. (2005). Major and trace element composition of the depleted MORB mantle (DMM). *Earth and Planetary Science Letters* **231**, 53-72.

Yilmaz, Y., Guner, Y. & Saroglu, F. (1998). Geology of the quaternary volcanic centres of the east Anatolia. *Journal of Volcanology and Geothermal Research* **85**, 173-210.

Zahedi, M. & Hajian, J. (1985). Sanandaj. Tehran: Geological Survey of Iran.

Zhang, Z. C., Xiao, X. C., Wang, J., Wang, Y. & Kusky, T. M. (2008). Post-collisional Plio-Pleistocene shoshonitic volcanism in the western Kunlun Mountains, NW China: Geochemical constraints on mantle source characteristics and petrogenesis. *Journal of Asian Earth Sciences* **31**, 379-403.

Zindler, A. & Hart, S. (1986). Chemical Geodynamics. *Annual Review of Earth and Planetary Sciences* **14**, 493-571.

Zou, H. B., Zindler, A., Xu, X. S. & Qi, Q. (2000). Major, trace element, and Nd, Sr and Pb isotope studies of Cenozoic basalts in SE China: mantle sources, regional variations, and tectonic significance. *Chemical Geology* **171**, 33-47.

Figure captions

Fig. 1. a) Distribution of late Cenozoic volcanic centres across the Arabia-Eurasia collision zone, superimposed on shaded digital topography. Iran political border shown by the fine dashed line. b) Late Cenozoic volcanic centres and active faults in Iran. Derived from Emami *et al.* (1993) and Walker *et al.* (2009). Lithosphere thickness contours from Priestley and McKenzie (2006). c) Main tectonic units of Iran and extent of main Eocene pre-collisional arc and back-arc magmatism (from Allen et al., 2011a). d) Location of samples and the extent of lava flows in the study area. Numbers refer to the locality numbers, which form the first part of the numeric component of the sample number.

Fig. 2. a) Total alkali versus SiO_2 plot for Kurdistan lavas. Divisions from Cox *et al.* (1979). b) MgO versus SiO_2; c) CaO versus SiO_2; d) TiO_2 versus SiO_2. All values as weight %.

Fig. 3. Normalised multi-element plots ("spidergrams") and REE plots. a) Primitivemantle normalised spidergrams for representative high and low La/Nb samples. Representative OIB and N-type MORB compositions from Sun and McDonough (1989). Shaded area represents the field of data for basic samples from the Qorveh and Bijar centres, except for outlying sample TBQ5.4. b) Spidergrams for potassic sample TBQ1.1 and outlying sample TBQ5.4. c) and d) Representative REE plots for samples from this study shown in Figs. 3a&b. Normalising values are from Sun and McDonough (1989).

Fig. 4. La v Nb plot for Quaternary lavas from Kurdistan. Fields for Ararat, Tendürek and Salmas and neighbouring minor centres in northwest Iran are from Kheirkhah *et al.* (2009) and references therein, only including rocks with MgO > 4% and SiO_2 < 60%. Triangles are basaltic lavas from Damavand volcano, from Liotard *et al.* (2008),

Mirnejad *et al.* (2010) and unpublished data, courtesy of Jon Davidson. Varto field from Pearce *et al.* (1990) and Buket and Temel (1998). Nemrut field from Pearce *et al.* (1990) and Özdemir *et al.* (2006). Karacadag field from Pearce *et al.* (1990), Sen *et al.* (2004) and Lustrino *et al.* (2010). The Varto, Nemrut and Karacadag fields use samples classified by these authors as basalt or alkali basalt. Bulk continental crust from Rudnick and Fountain (1995); GLOSS (Global Subducting Sediment) and Java trench average sediment from Plank and Langmuir (1998). Values are in ppm.

Fig. 5. a) Plot of La/Nb v La/Yb, showing that inferred smaller degree melts (high La/Yb) correlate with higher La/Nb. Ticked lines show mixing of end member TBQ20.1 with % values of GLOSS and Bulk continental crust; the overall trend of the Qorveh-Bijar samples shows no shift towards these crustal values. There is a trend towards OIB (composition from Sun and McDonough, 1989), but no sample lies close to the OIB ratios. b) Plot of La/Nb v Ni, indicating that the variation in La/Nb does not relate to the degree of fractionation of the samples. Ni values in ppm.

Fig. 6. La/Nb v Ti/Ti* ("Ti anomaly"), where Ti* is the extrapolated value of Ti based on the abundances of adjacent incompatible elements in the spidergram array. There is a broad correlation between La/Nb and Ti/Ti*, suggesting that variation in both parameters in the main Qorveh-Bijar sample set can be attributed to a common process.

Fig. 7. Isotope and combined isotope/elemental characteristics of lavas from Kurdistan Province. a) Plot of $^{143}Nd/^{144}Nd$ v $^{87}Sr/^{86}Sr$ for the Kurdistan samples, compared with other Quaternary basaltic rocks from NW Iran and late Cenozoic centres from eastern Turkey (Anatolia) (Kheirkhah *et al.*, 2009 and references therein). The samples in this study lie close to the bulk silicate Earth composition, with no samples close to the depleted character of Mt Ararat or the Kars plateau

centres (Fig. 1a). Mixing line shows % additions of Cretaceous Tethyan flysch sandstone sample 06FL03 from Serbia, from Prelević *et al.* (2008), and of GLOSS, from Plank and Langmiur (1998), to the depleted MORB mantle (DMM) of Workman and Hart (2005). Compositions for Enriched Mantle I (EM I) Enriched Mantle II (EM II) and HIMU reservoirs from Zindler and Hart (1986). Fields for OIB and Tibetan potassic lavas from Hart (1988) and Guo *et al.* (2006) respectively. b) Plot of $^{87}Sr/^{86}Sr$ v mg#. There is no significant correlation, and the single evolved sample (TBQ15.1) shows no higher $^{87}Sr/^{86}Sr$ than its basic counterparts. c) Plot of $^{87}Sr/^{86}Sr$ v Ce/Pb. The main sample array from Qorveh-Bijar shows no trend towards the composition of typical crustal sediments, such as GLOSS.

Fig. 8. Zr/Hf v Nb/Ta plot. Co-variance is interpreted as the joint control by garnet (on Zr/Hf) and rutile (on Nb/Ta) during partial melting. Modelled garnet peridotite melting curves are from Pfänder *et al.* (2007). See text for details. Compositions for chondrite, bulk silicate Earth, OIB and continental crust from Münker *et al.* (2003), with GLOSS and Javan trench sediment from Plank and Langmuir (1998).

Fig. 9. Rb/Sr v Ba/Rb plot. Schematic arrows indicate controls by phlogopite and amphibole during partial melting, after Furman and Graham (1999) and Tommasini *et al*. (2011). Note that the two highest Ba/Rb ratios are associated with samples where LOI > 1%; we suspect that these are affected by loss of Rb during weathering, and should be disregarded in this plot.

Fig. 10. a) Zr/Y v Nb plot and b) Zr/Y v Rb plot, highlighting that trace element data for the Qorveh-Bijar lavas do not fall on a simple linear mixing array between two distinct end-members. Nb and Rb values are in ppm.

Fig. 11. Non-modal batch melt model for Gd/Yb v Dy/Yb, using the equation of Shaw (1970). Ticks along curves indicate degree of melting in %. Two starting

compositions are shown: a fertile lherzolite of Fréménias *et al.* (2004), and a mixture of depleted MORB mantle source with 2% Tethyan flysch (Prelević *et al.*,2008; see Fig. 7a). Melting modes are from Thirlwall *et al.* (1994). Full parameters are given in Table 2. Results suggest melting in the garnet stability field for the great majority of samples, with the exception of TBQ5.4.

Fig. 12. Inferred tectonic setting and melting model for the Kurdistan lavas. Subducted Arabian plate oceanic and continental crust provides the source of a flux with the elemental signature of subduction, metasomatising overriding Eurasian lithosphere. Lithosphere thickening following initial continental collision takes mantle source regions downwards, across the backbend in the amphibole peridotite solidus curve (curve from Green and Falloon, 2005).

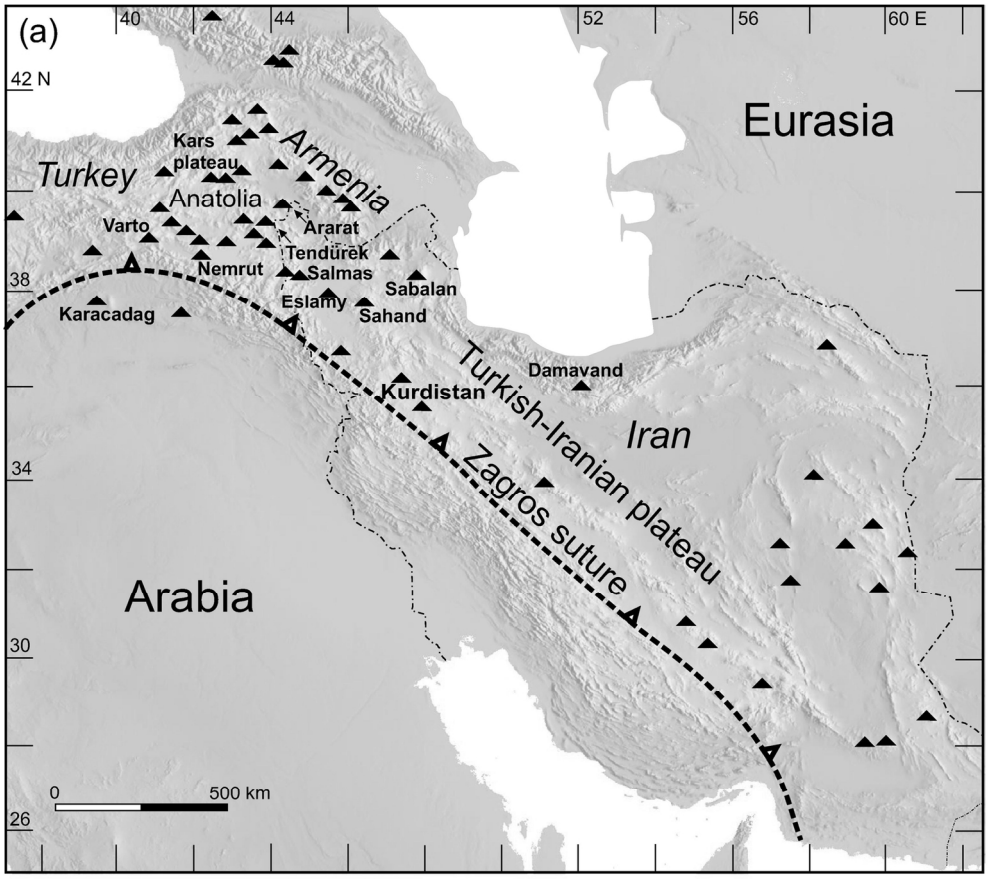

Figure 1a

147x144mm (300 x 300 DPI)

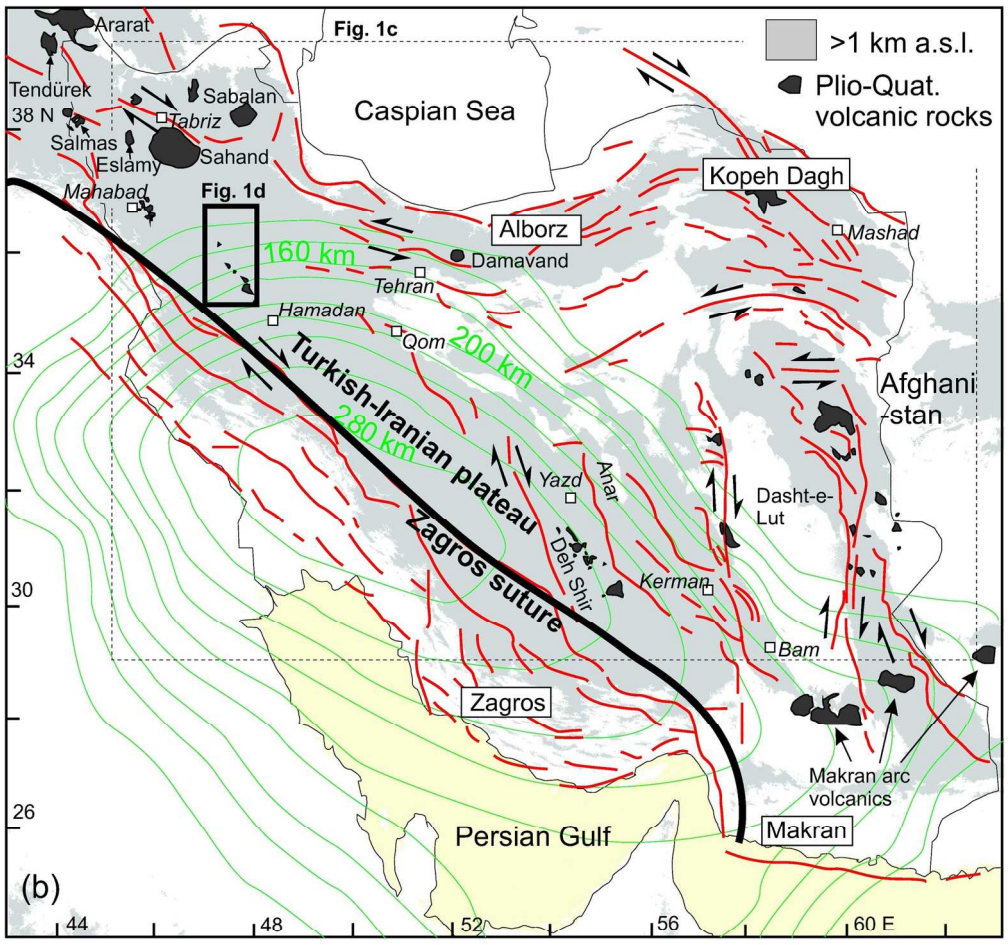

Figure 1b

155x159mm (300 x 300 DPI)

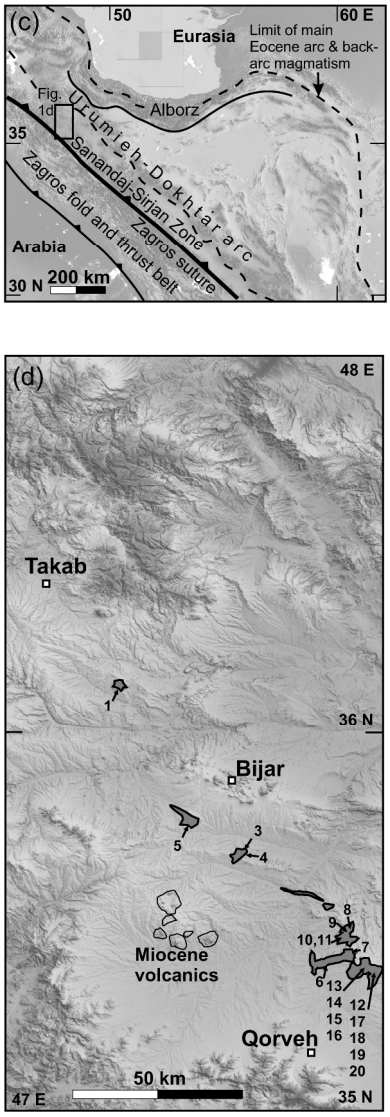

Figure 1c&d

229x711mm (300 x 300 DPI)

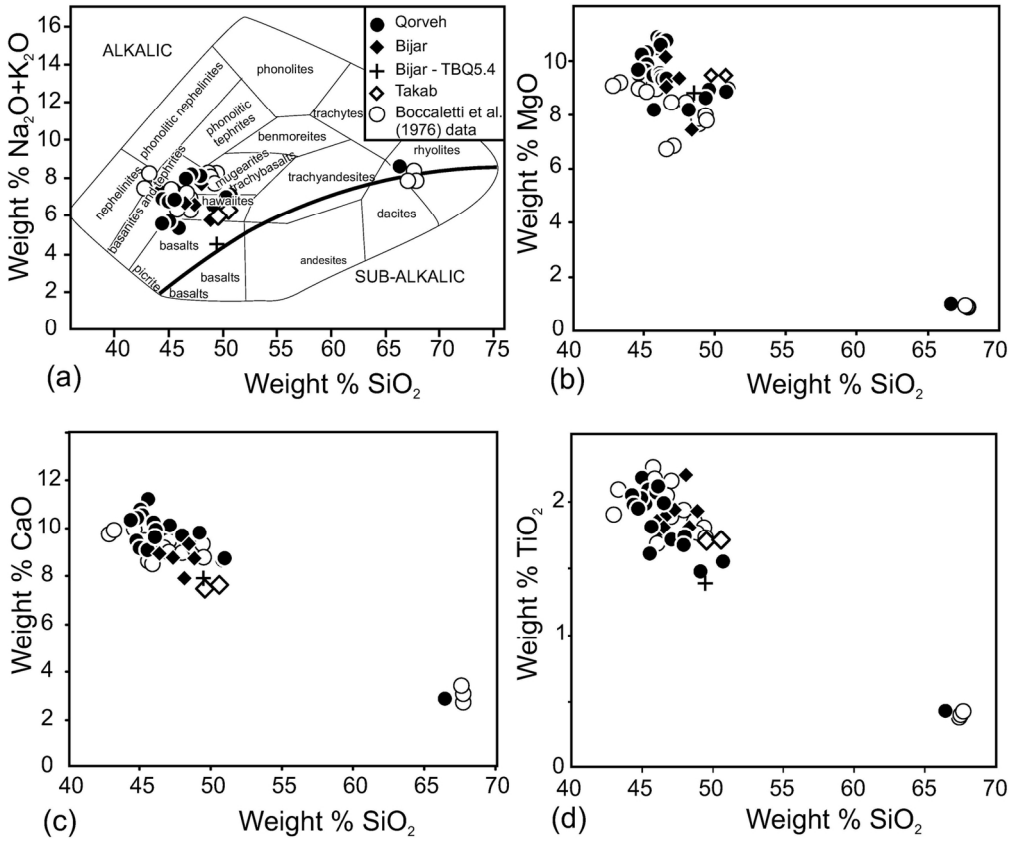

Figure 2

147x140mm (300 x 300 DPI)

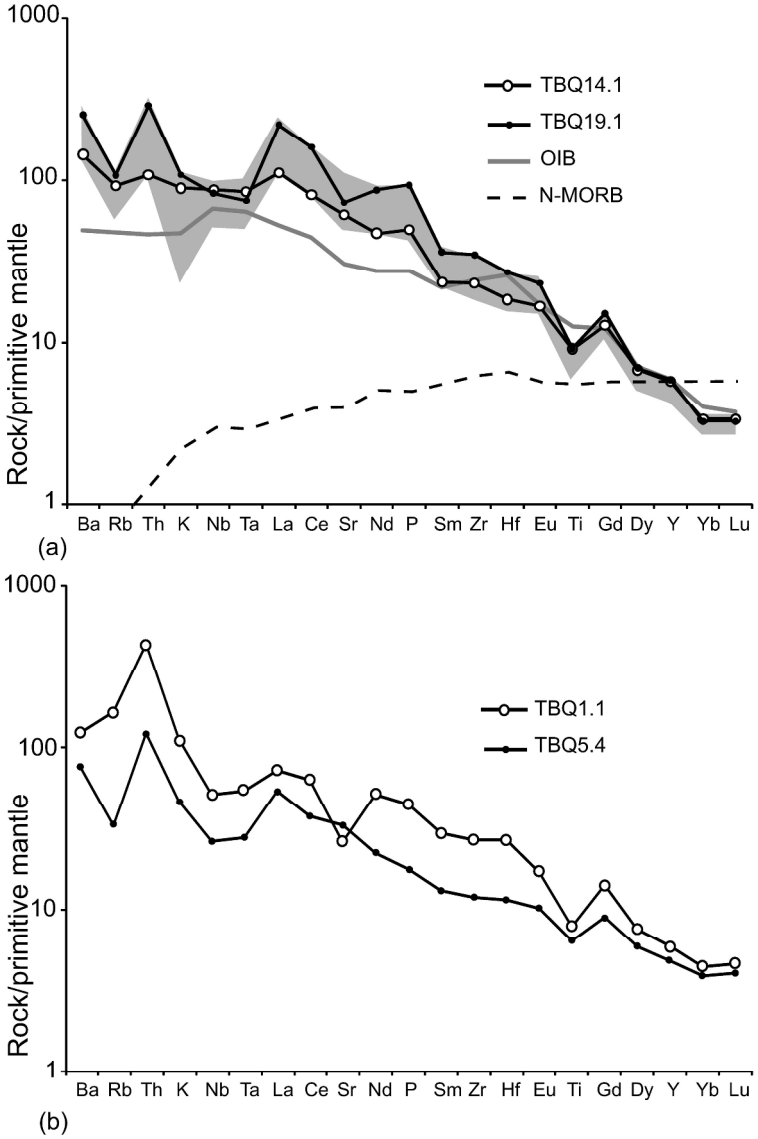

Figure 3a&b

245x392mm (300 x 300 DPI)

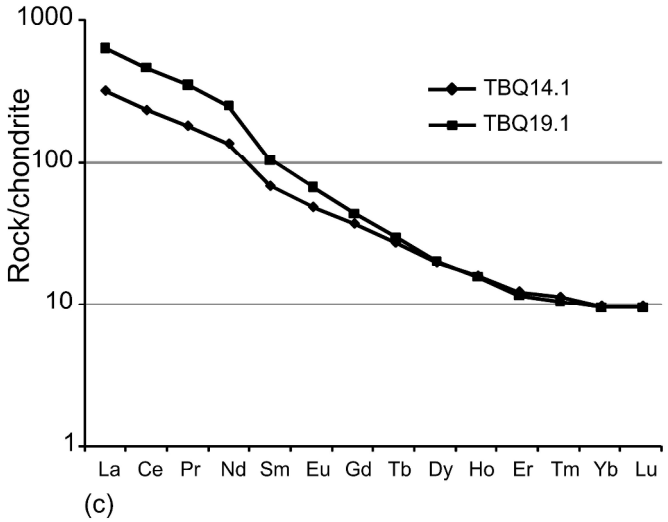

(c)

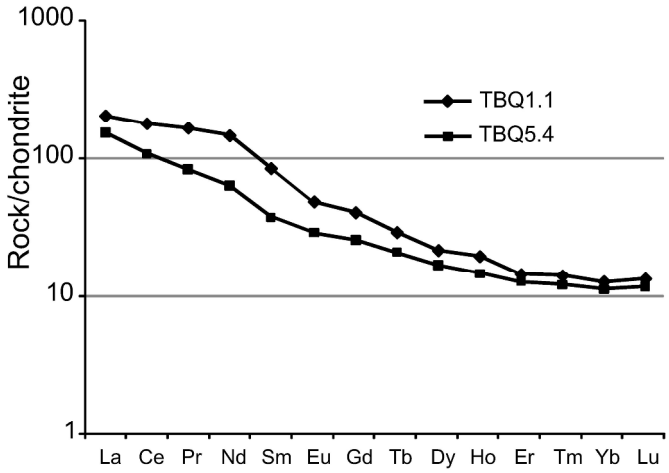

(d)

Figure 3c&d

231x420mm (300 x 300 DPI)

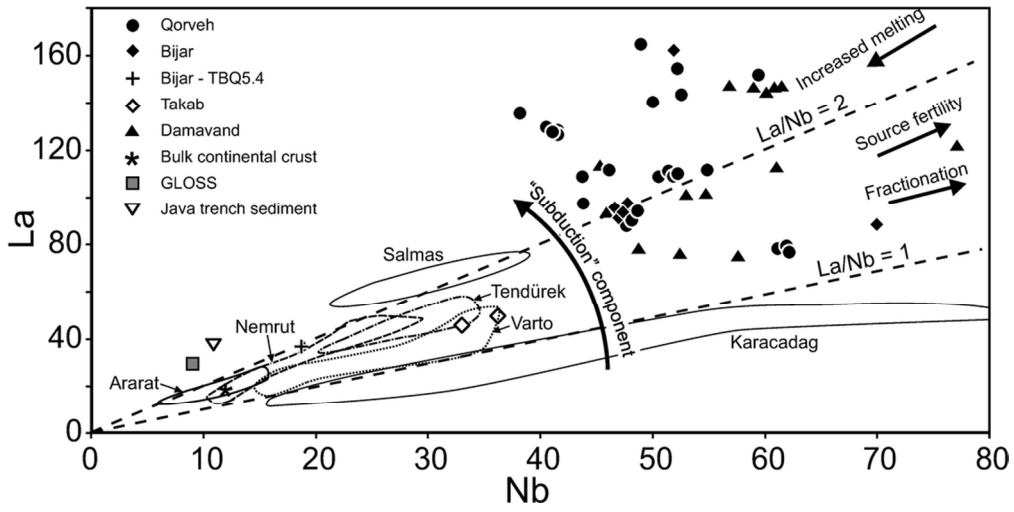

Figure 4

95x56mm (300 x 300 DPI)

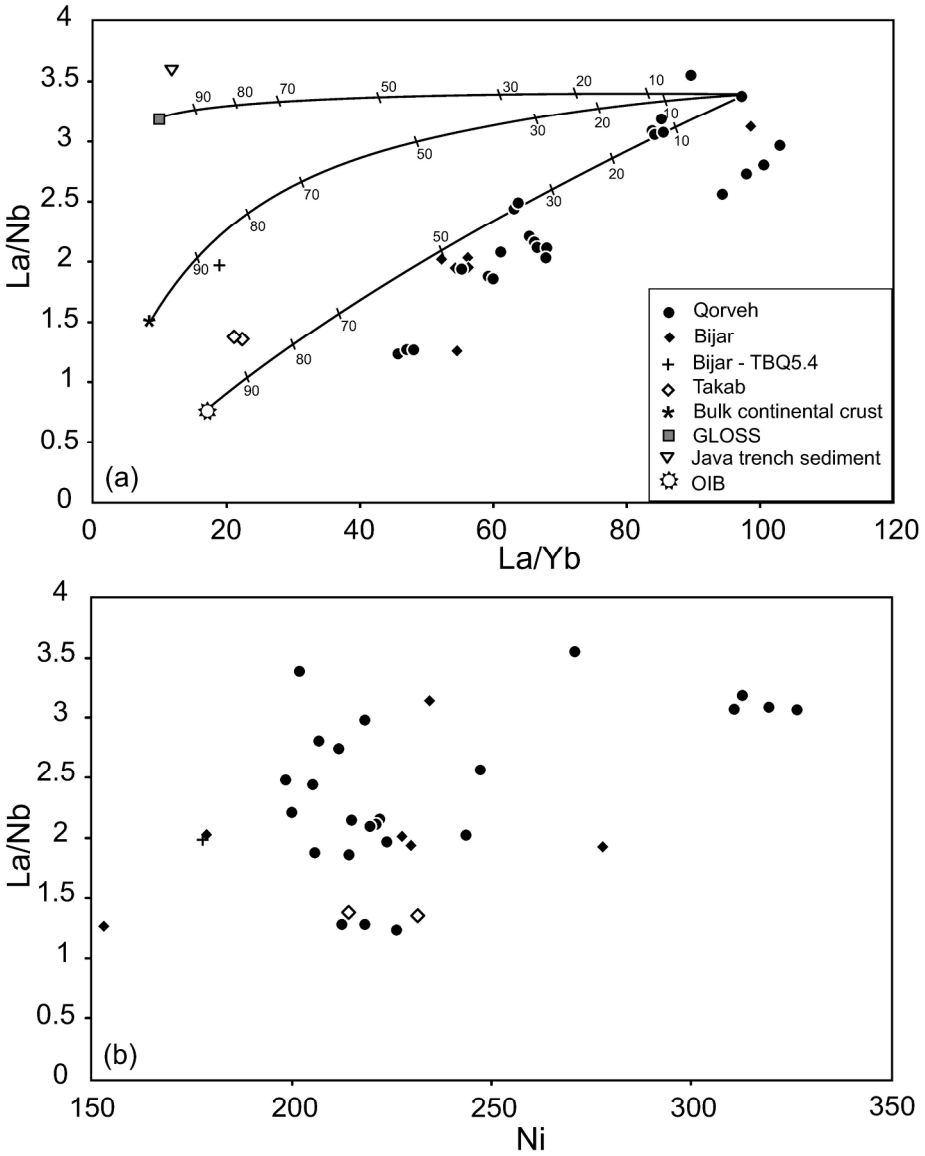

Figure 5

212x279mm (300 x 300 DPI)

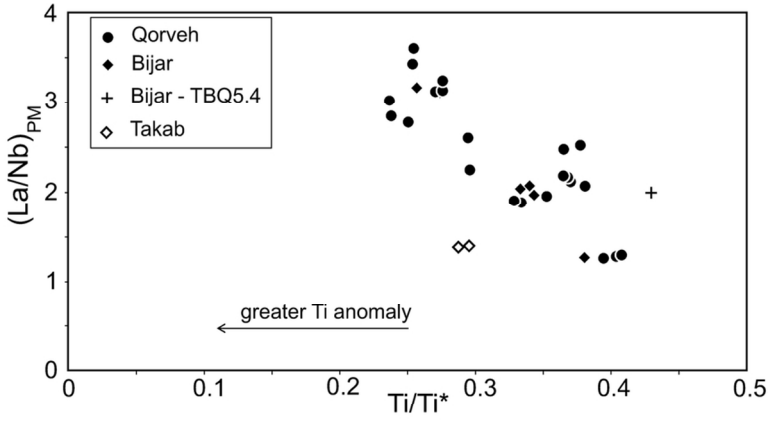

Figure 6

102x51mm (300 x 300 DPI)

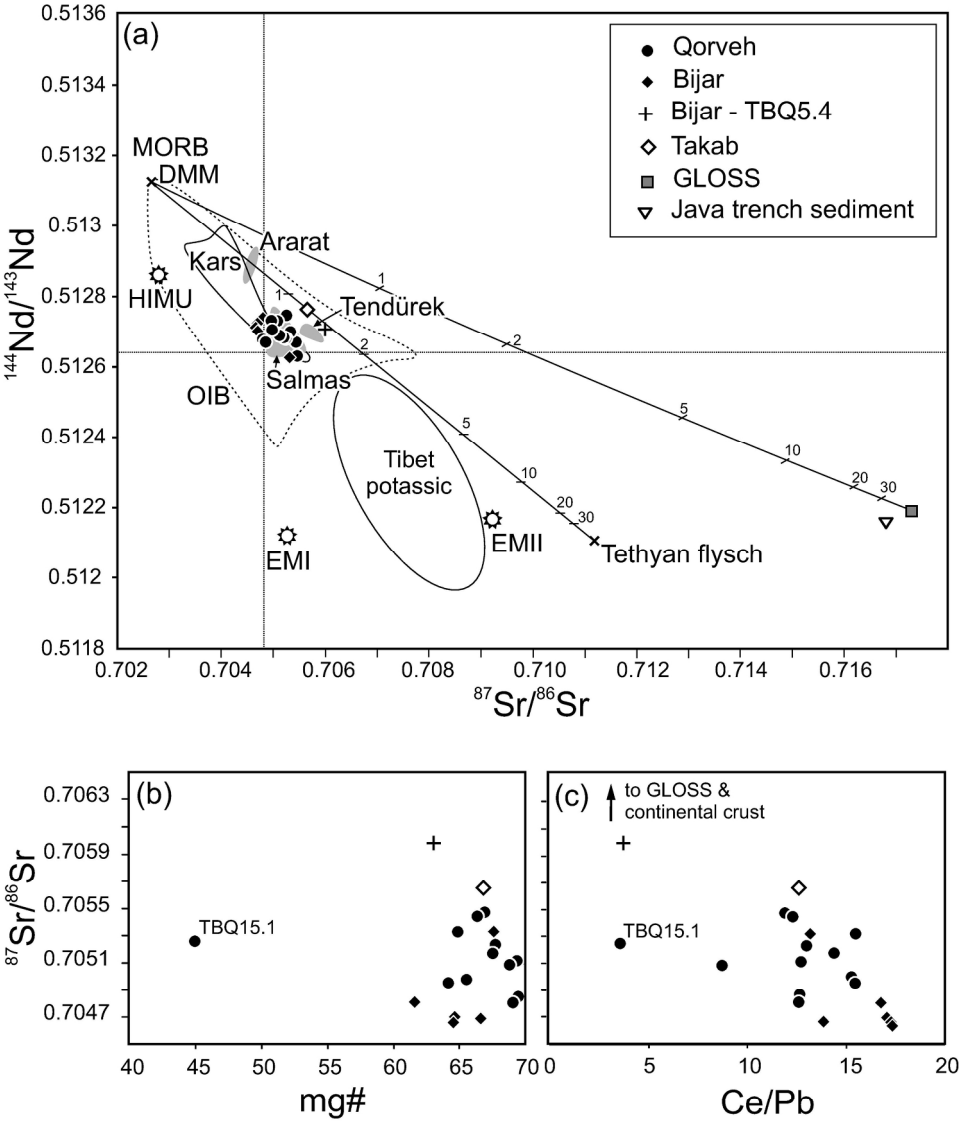

Figure 7

198x249mm (300 x 300 DPI)

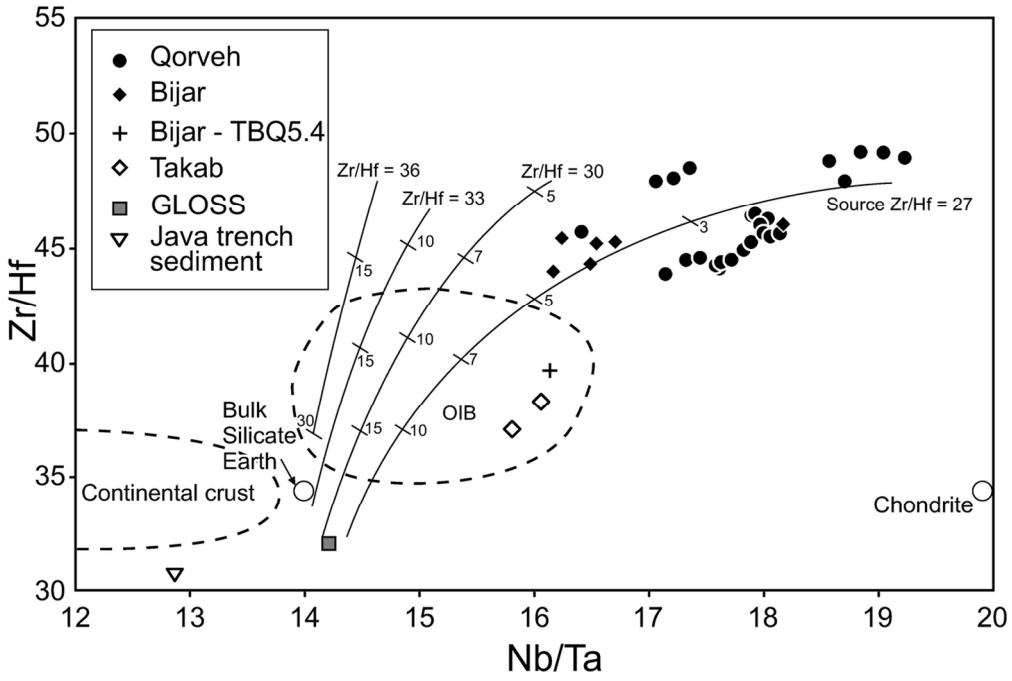

Figure 8

121x96mm (300 x 300 DPI)

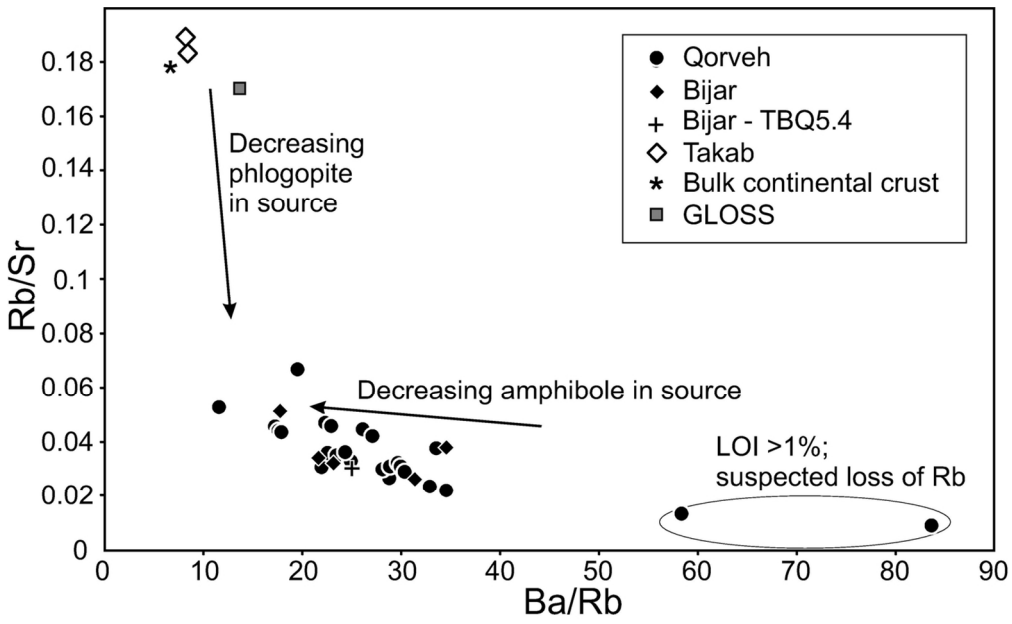

Figure 9

121x94mm (300 x 300 DPI)

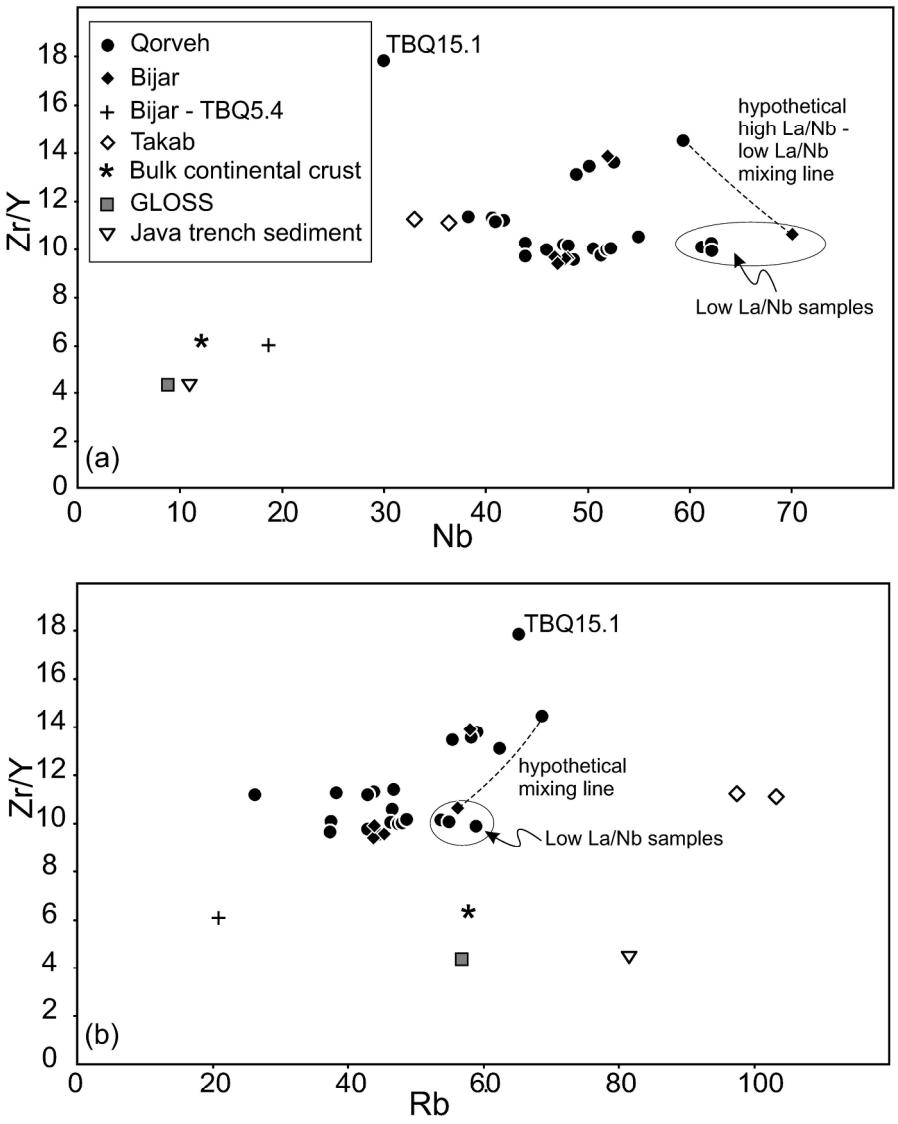

Figure 10

208x280mm (300 x 300 DPI)

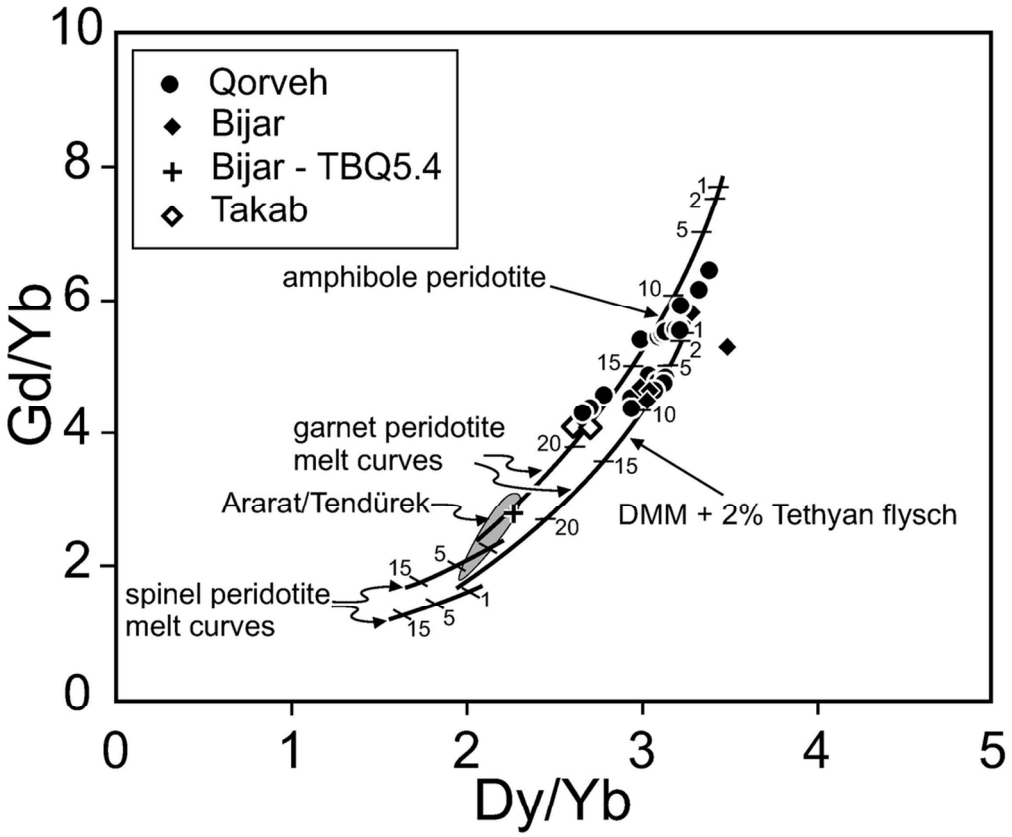

Figure 11

96x96mm (300 x 300 DPI)

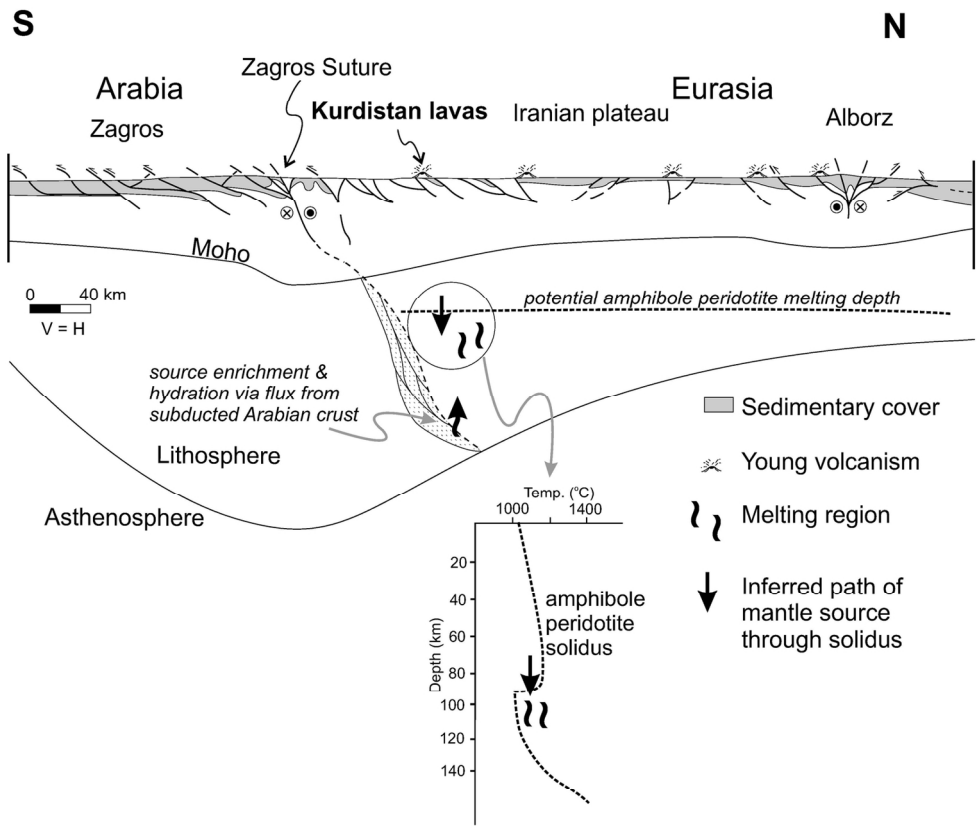

Figure 12

143x127mm (300 x 300 DPI)

Table 1: Major and trace element and Sr-Nd isotope data for Kurdistan lavas

Sample	TBQ1.1	TBQ1.2	TBQ3.4	TBQ4.1A	TBQ4.5A	TBQ4.6A	TBQ4.7
Lat.	36.118	36.118	35.683	35.693	35.693	35.693	35.683
Long.	47.308	47.308	47.617	47.627	47.627	47.627	47.617
SiO_2	49.57	50.58	48.19	48.88	47.35	46.49	46.43
TiO_2	1.70	1.71	2.19	1.92	1.92	1.87	1.84
Al_2O_3	13.27	13.37	14.93	14.77	14.08	13.72	13.50
Fe_2O_3	9.44	9.33	9.24	9.65	10.11	9.82	10.07
MnO	0.15	0.14	0.13	0.14	0.15	0.15	0.15
MgO	9.47	9.46	7.49	8.10	9.31	9.04	10.07
CaO	7.51	7.62	8.03	8.71	8.82	9.62	8.97
Na_2O	2.77	3.33	4.92	3.79	4.01	4.14	4.26
K_2O	3.33	3.06	2.93	2.06	2.68	2.67	2.38
P_2O_5	0.98	0.91	1.22	0.98	1.08	1.05	1.04
LOI	1.81	0.67	0.59	0.95	0.35	1.23	1.11
Total	100.00	100.20	99.88	99.94	99.85	99.82	99.82
Mg#	67	67	62	62	65	65	66
Trace elements (ppm)							
Sc	23.4	23.4	14.1	17.1	16.4	16.0	16.8
V	177	165	141	157	156	152	153
Cr	419	421	182	201	261	258	290
Co	37.8	37.9	32.4	37.4	40.0	39.1	43.5
Ni	232	214	153	178	227	224	278
Rb	103	97.3	56.3	37.3	44.0	45.3	43.9
Sr	547	532	1100	1445	1378	1334	1340
Y	26.9	25.8	25.7	25.7	24.2	23.8	24.0
Zr	299	291	273	247	232	228	226
Nb	36.3	32.9	70.0	46.8	47.9	47.6	46.9
Ba	852	826	1000	1172	1015	980	955
La	49.2	45.4	88.5	94.6	97.2	93.4	91.2
Ce	111	105	163	181	184	176	173
Pr	16.0	15.4	19.5	22.4	22.2	21.3	21.0
Nd	69.1	68.1	71.8	83.4	82.2	79.1	77.6
Sm	13.1	12.8	11.9	12.6	12.4	11.9	11.7
Eu	2.85	2.70	3.10	3.34	3.31	3.18	3.15
Gd	8.43	8.25	8.61	8.25	7.96	7.79	7.62
Tb	1.10	1.07	1.19	1.09	1.07	1.03	1.01
Dy	5.55	5.34	5.67	5.37	5.30	5.01	4.95
Ho	1.12	0.99	0.97	0.96	0.94	0.90	0.90
Er	2.41	2.33	2.09	2.17	2.13	2.02	2.02
Tm	0.36	0.36	0.29	0.33	0.29	0.29	0.28
Yb	2.19	2.15	1.63	1.82	1.73	1.66	1.68
Lu	0.34	0.33	0.23	0.27	0.25	0.24	0.24
Hf	7.80	7.84	6.00	5.58	5.27	5.04	4.98
Ta	2.26	2.08	4.31	2.84	2.96	2.88	2.80
Pb	11.9	8.3	9.7	13.8	10.7	10.2	12.4
Th	36.2	38.2	12.1	10.3	10.1	9.8	9.7
U	9.38	9.81	2.68	1.40	2.22	2.19	2.13
$^{143}Nd/^{144}Nd$		0.512764	0.512742		0.512727	0.512713	0.512705
$^{87}Sr/^{86}Sr$		0.705668	0.704806		0.704692	0.704666	0.704687

Table 1: Continued

Sample	TBQ5.4	TBQ5.11	TBQ6.1	TBQ7.1	TBQ7.2	TBQ7.3	TBQ7.4
Lat.	35.683	35.683	35.393	35.413	35.413	35.413	35.413
Long.	47.617	47.617	47.865	47.915	47.915	47.915	47.915
SiO_2	49.46	48.47	46.07	46.09	45.54	45.04	46.15
TiO_2	1.39	1.81	2.10	2.09	2.07	2.18	2.06
Al_2O_3	15.53	12.57	14.08	13.92	13.93	13.67	14.15
Fe_2O_3	10.34	8.40	10.16	10.06	10.03	10.34	10.03
MnO	0.15	0.12	0.14	0.14	0.14	0.14	0.14
MgO	8.94	8.79	9.48	9.60	9.44	10.23	9.40
CaO	7.93	9.33	9.30	9.10	9.11	9.22	8.91
Na_2O	3.17	4.64	4.52	4.21	4.21	4.26	4.80
K_2O	1.39	3.24	1.82	2.75	2.69	2.66	2.68
P_2O_5	0.39	1.73	1.40	1.40	1.41	1.50	1.35
LOI	1.65	0.17	0.94	0.74	1.04	0.69	0.23
Total	100.35	99.54	100.02	100.11	99.63	100.01	99.92
Mg#	63	67	65	65	65	66	65
Trace elements (ppm)							
Sc	21.6	15.1	16.3	16.2	15.5	16.0	15.5
V	160	137	165	163	157	163	158
Cr	342	267	292	292	286	310	271
Co	39.1	35.0	41.5	41.8	41.4	43.2	41.5
Ni	178	234	220	222	222	244	215
Rb	20.8	57.9	37.5	48.0	46.4	46.7	44.0
Sr	697	1534	1393	1352	1360	1323	1376
Y	21.9	24.6	23.9	23.9	23.5	23.9	24.1
Zr	133	341	242	240	236	252	238
Nb	18.7	52.0	52.2	52.0	50.6	54.9	51.4
Ba	521	2007	1080	1073	1082	1142	1098
La	36.8	163	110	109	109	112	110.8
Ce	66.5	301	206	204	204	207	206
Pr	8.0	35.4	24.3	24.2	23.9	24.3	24.1
Nd	30.0	126	87.5	87.2	86.4	87.9	87.3
Sm	5.8	17.0	12.9	12.8	12.7	12.8	12.6
Eu	1.71	4.16	3.26	3.26	3.22	3.34	3.28
Gd	5.34	9.15	7.84	7.78	7.78	8.00	7.82
Tb	0.79	1.16	1.05	1.05	1.05	1.06	1.06
Dy	4.34	5.30	5.14	5.03	5.05	4.99	5.09
Ho	0.84	0.91	0.90	0.89	0.89	0.89	0.89
Er	2.13	1.96	1.98	1.98	1.97	1.94	1.96
Tm	0.31	0.28	0.28	0.27	0.27	0.27	0.28
Yb	1.92	1.65	1.65	1.60	1.64	1.64	1.68
Lu	0.30	0.24	0.25	0.24	0.24	0.24	0.24
Hf	3.35	7.41	5.34	5.27	5.25	5.52	5.34
Ta	1.16	2.86	2.92	2.88	2.84	3.02	2.90
Pb	17.9	23.0	13.3	13.3	13.3	13.4	13.3
Th	10.3	26.4	13.7	13.7	13.5	14.7	13.6
U	2.58	4.44	2.73	2.83	2.78	2.79	2.85
$^{143}Nd/^{144}Nd$	0.512705	0.512665	0.512701	0.512707			
$^{87}Sr/^{86}Sr$	0.705998	0.705331	0.705331	0.704985			

Table 1: Continued

Sample	TBQ8.1	TBQ8.2	TBQ8.3	TBQ9.1	TBQ10.1	TBQ10.2	TBQ10.3
Lat.	35.454	35.454	35.454	35.480	35.479	35.479	35.479
Long.	47.922	47.922	47.922	47.914	47.908	47.908	47.908
SiO_2	44.80	45.13	45.04	45.96	46.25	46.14	46.13
TiO_2	1.95	1.99	2.01	1.81	1.79	1.80	1.79
Al_2O_3	13.25	13.62	13.61	12.57	12.71	12.76	12.78
Fe_2O_3	9.77	9.80	9.85	9.24	9.26	9.25	9.18
MnO	0.15	0.15	0.15	0.13	0.13	0.13	0.13
MgO	10.17	9.81	9.83	10.76	10.68	10.60	10.51
CaO	10.40	10.55	10.72	10.23	9.59	9.90	9.67
Na_2O	4.12	4.31	5.09	3.56	4.15	4.17	4.57
K_2O	2.78	2.74	0.72	1.84	3.06	3.04	2.05
P_2O_5	1.11	1.14	1.14	1.32	1.31	1.33	1.32
LOI	0.51	0.32	1.34	1.90	0.21	0.26	1.34
Total	99.23	99.70	99.60	99.39	99.44	99.65	99.63
Mg#	67	66	66	70	70	69	69
Trace elements (ppm)							
Sc	16.1	19.6	19.4	16.2	16.9	16.3	16.6
V	157	206	206	154	156	155	156
Cr	264	306	305	372	392	391	381
Co	40.7	42.2	41.5	41.3	42.3	42.0	41.6
Ni	230	205	198	313	327	320	311
Rb	45.1	47.7	43.0	38.1	43.3	43.6	26.2
Sr	1407	1455	1488	2382	1981	1999	2081
Y	24.7	23.6	23.1	22.5	23.0	22.9	23.1
Zr	236	236	227	254	257	257	260
Nb	48.6	46.1	43.8	40.6	41.5	41.4	41.6
Ba	985	1409	1300	1554	1493	1508	1527
La	94.0	112	109	129	127	128	128
Ce	179	211	206	257	253	253	255
Pr	21.7	25.0	24.5	31.9	31.6	31.5	31.5
Nd	80.1	88.8	88.0	118	117	116	117
Sm	12.2	12.6	12.4	16.1	16.0	16.0	16.0
Eu	3.28	3.09	3.03	3.97	3.96	3.99	3.96
Gd	7.77	7.29	6.98	8.26	8.36	8.40	8.30
Tb	1.06	0.96	0.95	1.03	1.04	1.04	1.05
Dy	5.17	4.63	4.62	4.69	4.80	4.76	4.73
Ho	0.92	0.86	0.83	0.82	0.84	0.82	0.82
Er	2.08	1.96	1.95	1.77	1.81	1.77	1.79
Tm	0.29	0.29	0.29	0.25	0.25	0.26	0.26
Yb	1.69	1.78	1.71	1.52	1.51	1.52	1.50
Lu	0.25	0.27	0.27	0.21	0.22	0.22	0.23
Hf	5.15	5.12	4.97	5.79	5.79	5.79	5.83
Ta	2.96	2.56	2.43	2.37	2.36	2.39	2.39
Pb	10.6	17.5	16.7	20.2	20.0	20.0	20.4
Th	10.0	19.1	18.2	14.4	14.4	14.4	14.5
U	2.16	3.53	2.73	2.75	2.83	2.82	2.82
$^{143}Nd/^{144}Nd$			0.512672	0.512689	0.512669		
$^{87}Sr/^{86}Sr$			0.705447	0.705119	0.704859		

Table 1: Continued

Sample	TBQ11.1	TBQ12.2	TBQ13.1	TBQ13.2	TBQ14.1	TBQ14.2	TBQ15.1
Lat.	35.467	35.370	35.365	35.365	35.396	35.396	35.393
Long.	47.898	47.978	47.974	47.974	47.955	47.955	47.962
SiO_2	46.56	49.19	47.13	48.00	44.45	44.84	66.44
TiO_2	1.81	1.46	1.72	1.67	1.98	2.01	0.44
Al_2O_3	12.60	12.70	12.76	12.87	13.36	13.58	16.48
Fe_2O_3	9.46	7.71	8.02	7.87	10.53	10.70	2.55
MnO	0.13	0.12	0.12	0.12	0.16	0.16	0.05
MgO	10.67	8.62	8.39	8.18	9.54	9.61	1.06
CaO	9.50	9.82	10.08	9.69	9.84	9.46	2.92
Na_2O	3.81	4.01	4.96	4.89	4.65	4.50	5.67
K_2O	3.18	2.64	3.35	3.37	2.69	2.64	3.08
P_2O_5	1.29	1.07	1.71	1.61	1.09	1.12	0.24
LOI	0.36	2.13	0.29	0.25	1.20	1.03	1.21
Total	99.55	99.57	99.42	99.25	99.71	99.86	100.14
Mg#	69	69	67	67	64	64	45
Trace elements (ppm)							
Sc	17.0	14.1	13.7	13.7	19.4	17.8	2.5
V	161	135	136	136	190	185	32
Cr	367	343	235	253	273	261	8
Co	42.8	32.6	34.4	33.7	45.6	43.8	5.2
Ni	271	200	219	212	227	218	8
Rb	46.5	48.7	59.0	58.0	59.0	55.0	65.4
Sr	2002	1158	1912	1869	1293	1278	970
Y	23.8	20.7	24.1	24.0	26.3	25.3	12.2
Zr	270	212	332	327	260	254	218
Nb	38.3	43.9	52.1	52.5	62.2	61.2	29.8
Ba	1530	1323	1759	1656	1011	967	1288
La	136	97.3	155	144	76.6	78.0	61.7
Ce	274	184	296	273	144	147	101
Pr	34.8	21.8	35.4	32.5	17.4	17.6	10.5
Nd	129	78.2	128	117	64.0	65.1	33.7
Sm	17.5	11.3	17.7	16.1	10.4	10.4	4.6
Eu	4.37	2.79	4.35	4.02	2.80	2.84	1.15
Gd	8.82	6.82	9.29	8.67	7.60	7.29	2.69
Tb	1.09	0.88	1.13	1.05	1.02	1.01	0.39
Dy	4.98	4.13	5.01	4.71	5.02	4.88	2.00
Ho	0.86	0.74	0.83	0.80	0.90	0.89	0.38
Er	1.86	1.67	1.77	1.72	2.04	1.99	0.99
Tm	0.26	0.24	0.24	0.24	0.29	0.28	0.15
Yb	1.52	1.49	1.51	1.47	1.66	1.66	1.01
Lu	0.23	0.23	0.21	0.22	0.25	0.25	0.17
Hf	6.13	4.77	6.94	6.65	5.35	5.27	4.70
Ta	2.17	2.49	2.79	2.76	3.58	3.55	1.66
Pb	21.6	20.6	20.6	22.7	9.4	8.7	27.7
Th	14.5	19.6	24.8	24.6	9.2	9.3	23.4
U	2.93	4.44	4.30	4.43	2.39	2.37	5.29
$^{143}Nd/^{144}Nd$	0.512678		0.512683		0.512731		0.512749
$^{87}Sr/^{86}Sr$	0.704809		0.705179		0.704958		0.705259

Table 1: Continued

Sample	TBQ16.1	TBQ17.1	TBQ17.2	TBQ18.1	TBQ19.1	TBQ20.1
Lat.	35.399	35.376	35.376	35.355	35.355	35.533
Long.	47.893	47.989	47.989	47.973	47.973	47.842
SiO_2	44.46	50.73	50.84	45.57	46.58	48.16
TiO_2	2.02	1.55	1.55	1.61	1.99	1.74
Al_2O_3	13.44	13.12	13.14	12.39	12.08	13.07
Fe_2O_3	10.79	7.95	8.01	7.78	8.85	8.30
MnO	0.16	0.12	0.12	0.11	0.13	0.12
MgO	9.48	8.86	8.99	8.21	9.27	8.48
CaO	10.38	8.64	8.66	11.27	9.74	9.32
Na_2O	4.45	4.23	4.42	4.40	4.78	4.45
K_2O	1.19	2.81	2.78	3.28	3.26	3.32
P_2O_5	1.17	1.07	1.08	1.64	2.06	1.53
LOI	1.92	0.75	0.34	2.15	0.23	0.78
Total	99.59	99.85	99.95	99.28	99.32	99.45
Mg#	64	69	69	68	67	67
Trace elements (ppm)						
Sc	17.4	15.7	15.9	13.4	15.9	15.5
V	182	157	154	132	151	148
Cr	265	367	368	175	272	271
Co	43.6	34.9	35.3	33.8	37.6	35.1
Ni	213	206	214	207	247	202
Rb	11.6	55.0	53.9	55.5	68.6	62.4
Sr	1408	1182	1169	1859	1534	1676
Y	25.5	22.0	21.7	23.6	26.8	26.6
Zr	262	221	221	317	389	348
Nb	62.1	48.1	47.7	50.1	59.4	48.9
Ba	964	1230	1227	1561	1780	2097
La	79.0	90.3	88.8	140	152	165
Ce	149	171	169	268	286	301
Pr	17.8	20.2	20.1	32.2	33.5	34.6
Nd	65.7	73.5	72.4	117	118	121
Sm	10.3	10.7	10.4	16.3	16.0	16.3
Eu	2.83	2.68	2.61	4.02	3.89	3.95
Gd	7.66	6.56	6.48	8.99	8.97	9.18
Tb	1.02	0.83	0.85	1.07	1.11	1.12
Dy	4.93	4.06	3.99	4.72	5.14	5.06
Ho	0.89	0.74	0.71	0.79	0.89	0.90
Er	1.99	1.68	1.69	1.66	1.92	1.96
Tm	0.28	0.25	0.24	0.24	0.27	0.29
Yb	1.64	1.53	1.48	1.40	1.61	1.70
Lu	0.24	0.23	0.22	0.22	0.24	0.26
Hf	5.47	4.78	4.75	6.49	7.90	7.14
Ta	3.64	2.66	2.66	2.61	3.15	2.63
Pb	10.0	19.6	19.4	20.7	20.4	25.2
Th	9.2	18.4	18.3	23.2	24.8	27.1
U	2.44	4.14	4.12	4.08	4.22	4.51
$^{143}Nd/^{144}Nd$		0.512732		0.512679		0.512633
$^{87}Sr/^{86}Sr$		0.705081		0.705243		0.705472

Table 2: Partition coefficients and compositions used in trace element modelling of samples from Kurdistan Province (Fig. 11).

	Gd	Dy	Yb
Ol	0.0012	0.004	0.023
Opx	0.04	0.06	0.1
Cpx	0.4	0.38	0.4
Sp	0.0006	0.0015	0.0045
Gt	3.13	7.52	17.2
Amph	0.018	0.014	0.102
Rut	0.01	0.012	0.012

Partition coefficients from Kelemen *et al.* (1993), Tiepolo *et al.* (2003) and Foley (2008).

Initial composition, garnet peridotite: 56.8% olivine, 21.1% opx, 7.6% cpx, 11.5% garnet; 2.5% amphibole; 0.5% rutile (modified from Thirlwall *et al.* (1994).

Melt proportions: 5% olivine, 19% opx, 28% cpx, 42% garnet; 6% amphibole; 0.1% rutile.

Initial composition, spinel peridotite: 54.8% olivine, 27% opx, 11.9% cpx, 3.3% spinel; 2.5% amphibole; 0.5% rutile.

Melt proportions: 9% olivine, 25% opx, 48% cpx, 12% spinel; 6% amphibole; 0.1% rutile.

Initial abundances, amphibole peridotite sample 98-08 of Fréménias *et al.* 2004 (ppm): Gd – 0.66, Dy – 0.66, Yb- 0.43.

Initial abundances, DMM of Workman and Hart (2005) mixed with 2% Serbian flysch sample 06FL03 of Prelević *et al.* (2008) (ppm): Gd – 0.446, Dy – 0.587, Yb- 0.406.